Sustainable desalination schemes for climate change adaptation

Master thesis presented by Víctor Puchal Bosch
to obtain the Master degree in Chemical Engineering
from the Universitat Rovira i Virgili

Company Supervisor: Carmen Torres Costa
URV Tutor: Manuel Martínez Del Álamo

Tarragona, June 2024

UNIVERSITAT ROVIRA I VIRGILI etsEQ Escola Tècnica Superior d'Enginyeria Química

Approval for MASTER'S THESIS defence	
Master: Master's degree in chemical engineering *MASTER'S THESIS Title: Sustainable desalination schemes for climate change adaptation* *ACADÈMIC Year: 2023-2024*	
Student: Víctor Puchal Bosch	
ACADÈMIC MT SUPERVISOR: Manuel Martínez Del Álamo. *Email: manuel.martinezd@urv.cat.*	
Approval Academic Supervisor:	
Dr. Manuel Martínez Del Álamo in his capacity as MT supervisor, he states that he considers that the MT: *X It is appropriate and consequently recommends its defence* *☐ It does not recommend its defence as it has shortcomings, which are set out in the attached document*	
Signature: 	*Date:* *10/06/24*
STATEMENT OF ABSENCE OF CONFLICT OF CONFIDENTIALITY	
Dr. Carmen Torres Costa, in her capacity as external tutor (*) of the MT, states that she has reviewed the content of the MT and that the public version of the MT it does not contain any information that can be considered confidential by the company *(*) In the case that MT is not external, this section will be filled in by the academic supervisor*	
Signature: 	*Date:* *10/06/24*

Acknowledgements

First of all, I would like to give special thanks to Dra. Carmen Torres Costa and Dr. Manuel Martínez Del Álamo for their support in carrying out this project. In addition, I would also like to express my gratitude to all the staff at Eurecat for offering me the possibility of doing this internship at their facilities, learning first-hand what it is like to carry out a research-focused project. In this case, with a view to desalination, a technology that is becoming increasingly relevant in the society and industry.

Table of contents

Nomenclature

Parameter	Description	Units
$a_{w,f}$	Activity coefficient for an aqueous solution of sodium chloride	$-$
X_m	Average value	$-$
k_B	Boltzmann's constant	J/K
L	Channel length	m
σ_v	Collision diameter of water vapor molecules	m
α	Contribution from Molecular to Knudsen diffusion	$-$
$PD_{w,a}$	Diffusivity of the water vapors	$Pa \cdot m^2/s$
Q_m	Energy flux across the membrane	W/m^2
Q_f	Energy flux on the feed side of the membrane	W/m^2
Q_p	Energy flux on the permeate side of the membrane	W/m^2
Q_c	Energy flux transferred by conduction	W/m^2
Q_v	Energy flux transferred by phase change	W/m^2
Δh_v	Enthalpy of vaporization	kJ/kg
D_e	Equivalent diffusion coefficient	s/m
c_f	Feed stream concentration	kg/m^3
ν	Fluid cinematic viscosity	$m^2/\,s$
ρ	Fluid density	kg/m^3
μ	Fluid dynamic viscosity	$Pa \cdot s$
μ_f	Fluid dynamic viscosity at feed temperature	$Pa \cdot s$
$\mu_{m,f}$	Fluid dynamic viscosity at membrane-feed temperature	$Pa \cdot s$
$\mu_{m,p}$	Fluid dynamic viscosity at membrane-permeate temperature	$Pa \cdot s$
μ_p	Fluid dynamic viscosity at permeate temperature	$Pa \cdot s$
A_c	Fluid flow passage area	m^2
u	Fluid velocity	m/s
λ	Free path	$-$
U	Global heat transfer coefficient	$W/(m^2 \cdot K)$
C_p	Heat capacity	$J/(kg \cdot K)$
h	Heat transfer coefficient	$W/(m^2 \cdot K)$
h_f	Heat transfer coefficient on the feed side of the membrane	$W/(m^2 \cdot K)$
h_p	Heat transfer coefficient on the permeate side of the membrane	$W/(m^2 \cdot K)$
D_h	Hydraulic diameter	m
R_{gas}	Ideal gas constant	$J/(kmol \cdot K)$

D_k	Knudsen diffusion coefficient	s/m
Kn	Knudsen number	$-$
J_w	Mass flow rate across the membrane	$kg/(m^2 \cdot s)$
σ_v	Mean deviation	$-$
T_m	Mean membrane temperature	K
k_m	Membrane conductivity	$W/(m \cdot K)$
$\beta_{pol-vap}$	Membrane conductivity parameter	$-$
k_{pol}	Membrane polymer conductivity	$W/(m \cdot K)$
ε	Membrane porosity	$-$
δ_m	Membrane thickness	m
τ	Membrane tortuosity	$-$
k_{vap}	Membrane vapors conductivity	$W/(m \cdot K)$
$x_{Nacl,f}$	Molar fraction of sodium chloride on the feed side of the membrane	$-$
D_m	Molecular diffusion coefficient	s/m
MW_{H2O}	Molecular weight of water	$kg/kmol$
Nu	Nusselt number	$-$
$P_{air,pore}$	Partial pressure of air inside the membrane pores	Pa
$P_{w,v,p}$	Partial pressure of water vapors inside the membrane pores	Pa
c_p	Permeate stream concentration	kg/m^3
π	Pi number	$-$
d_{pore}	Pore diameter	m
Pr	Prandtl number	$-$
p_f	Pressure at the feed stream	Pa
p_p	Pressure at the permeate stream	Pa
Re	Reynolds number	$-$
R	Salt rejection factor	%
R_f	Split ratio on the feed loop	$-$
R_p	Split ratio on the permeate loop	$-$
σ	Standard deviation	$-$
$T_{m,f}$	Temperature at the membrane-feed side of the membrane	K
$T_{m,p}$	Temperature at the membrane-permeate side of the membrane	K
T_f	Temperature of the feed stream	K
T_p	Temperature of the permeate stream	K
k	Thermal conductivity	$W/(m \cdot K)$
ε_t	Total error	$-$
P_{pore}	Total pressure inside the membrane pores	Pa
$p^0_{m,f}$	Vapor pressure on the feed side of the membrane	Pa

$p^0_{m,f,c}$	Vapor pressure on the feed side of the membrane corrected	Pa
$p^0_{m,p}$	Vapor pressure on the permeate side of the membrane	Pa
$\dot{v}$	Volumetric flow rate	m^3/s
P	Wet perimeter	m

Summary

Due to population growth, climate change and the use of water in countless applications, obtaining water from natural sources such as rivers or reservoirs is becoming increasingly scarce. The rise in global temperature is affecting the climate, causing severe periods of drought and lack of water in different countries. Currently, there is great interest in the search for methods or technologies that allow to obtain water suitable for consumption in the most sustainable, economical and efficient way.

In this project, a numerical study of one of the relatively new desalination technologies, Direct contact membrane distillation (DCMD), is carried out. A series of hypotheses and simplifications have been established when developing the model. The results obtained were then successfully validated with experimental results available in the literature, and the accuracy of the model was determined. In the validation process, the thermodynamic properties considered initially were those of pure water and then the procedure was repeated using correlations, which estimate the thermodynamic properties as a function of temperature and salinity.

Once the model had been validated, it was implemented in the DWSIM chemical process simulator using the Python programming language. In the code itself, the information relationship between the material flows and the variables defined in the mathematical model has been established. In addition, the multivariable Newton-Raphson method has been used to solve the system of non-linear equations posed by the model. Different sensitivity analyses have been carried out to optimize the operating conditions from an energy point of view. For the most favorable operating conditions studied, the energy consumption of the process is 0.420 kWh per kilogram of desalinated water with a concentration of 38 g/L (approximately that of the Mediterranean Sea).

Finally, by dimensioning a possible pilot desalination plant with the current characteristics, the desalination process was simulated, but this time considering the head loss in the elbows and in the pipes of the system, in addition to the loss of energy released from the pipes by convection and radiation. The results obtained for this case are very similar to those obtained previously, in which pipe friction and energy loss to the environment have not been considered. It can therefore be affirmed that for the specific characteristics and dimensions of the process studied, these factors can be considered as negligible.

1. Introduction

1.1. Background

Water is an essential resource in nowadays society, it is used for a wide variety of applications as well as for personal consumption. In the industry, the largest consumers are chemical, agriculture-food, metallurgy, textile, paper and mineral industries. The chemical sector itself accounts for 25% of industrial water consumption [1].

On the other hand, population growth is steadily increasing water demand despite the consequences of climate change. The progressive increase of the global temperature is giving rise to periods of drought in a significant number of countries, which are becoming increasingly severe and long-lasting. According to a study carried out by the United Nations (UN), the number and duration of droughts has increased by 29% since 2000 [2].

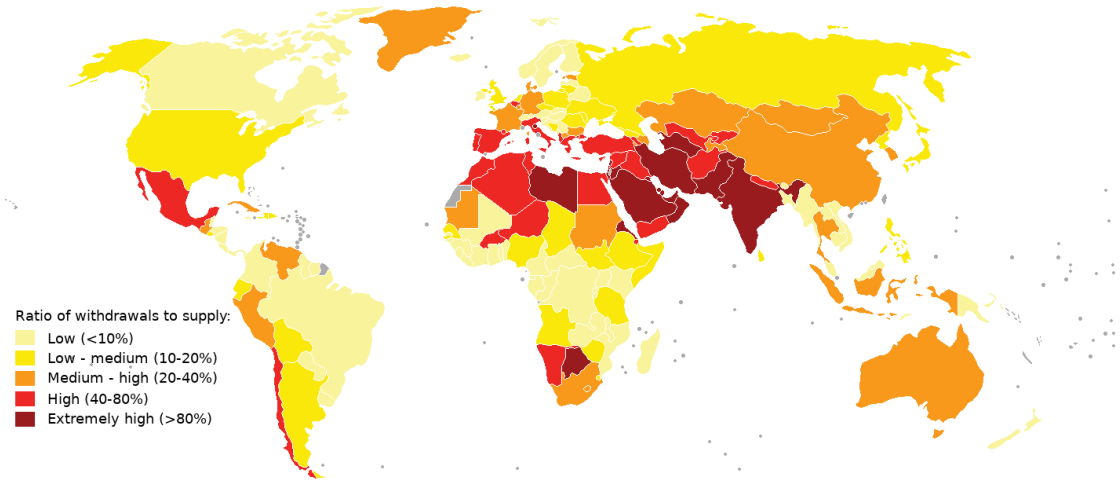

Figure 1.1. Map of global water stress ratio of water used relative to water availability, 2019 [3].

Countries or regions that are more isolated or less well communicated with neighboring populations are the most vulnerable in these cases. Furthermore, in the case of developing countries that do not have the necessary resources to have safe water consumption conditions, there is a risk of contracting diseases.

According to the United States Environmental Protection Agency (EPA), water pollution sources are divided into two types, chemical and microbiological

contaminants [4]. Where 90 different types of contaminants have to be exhaustively controlled in order to declare drinking water [5].

The UN has set the goal of ensuring universal access to safe drinking water by 2030. Of the 17 sustainable development goals, number 6 refers to Clean water and sanitation. A total of 6 targets have been established to be able to guarantee access to drinking water for everyone, with safe hygienic conditions, thus eliminating possible contaminating agents. It also includes the development of water- and sanitation-related activities as well as the restoration of water-related ecosystems [6].

The UN targets are promising; however, the current situation is far from what is expected to be achieved by 2030. The following image shows some of the data collected in the reports of recent years.

Figure 1.2. United Nations infographic about the 6th sustainable development goal, Clean water and sanitation, 2023 [6].

The results of the studies carried out show that in the year 2022 about 2.2 billion people did not have access to safe drinking water with the recommended hygienic conditions. That corresponds to a 27.7 % of the world's population [7].

Some countries have begun to adapt to the new times of drought. There are technologies (desalination techniques) that make it possible to obtain water suitable for human consumption from the largest available source, the sea. Where it is estimated that 97.5% of the water present on planet Earth is found. The remaining 2.5% is non-saline water, 70% of which is in the form of ice or snow, and 30% in rivers, lakes and as vapor in the atmosphere [8].

It should be taken into account that drinking sea water directly can cause serious health problems due to the high concentration of salt. The amount of salt can vary according to different regions or oceans.

Table 1.1. Salt concentration depending on different oceans [8].

Seawater source	Salt concentration [g/L]
Pacific	33.5
Atlantic	33.5
Caribbean	36.0
Mediterranean	38.0
Indian	40.0
Red sea	41.0
Arabian Gulf	45.0

The difference in salinity in different regions is due to a number of factors, including climate temperature, ocean currents, winds and freshwater flows. In warmer areas, the sun evaporates more water at the surface, and the salt, which does not evaporate, remains in the ocean itself, increasing its salinity.

The presence of rivers also affects the salinity of the ocean, the fresh water that flows into the ocean decreases the concentration of salt. On the other hand, wind and mainly marine currents have a significant influence on the distribution of salinity in the different oceans.

1.2. Desalination technology

Desalination technologies are those that, by means of separation techniques, make it possible to reduce the salt concentration of a saltwater or seawater source almost completely, where most of the extracted salt is concentrated in a single process output stream, known as rejected brine.

Therefore, in desalination processes, there is an input to the desalination system, which is always a feed stream with a certain salt concentration. In the feed solution, the water acts as solvent and the salt as solute. Ideally, the objective is to separate the 100% of the salt from the water in order to have a stream of only water as a product for its later use or consumption.

To carry out the separation, energy is required to be supplied to the system, either thermal, mechanical or electrical. As a result of the separation, there are two resulting streams, one with a salt concentration below the feed stream (product), and the other with a higher concentration (rejected brine). The following image shows conceptually the principle of a desalination process.

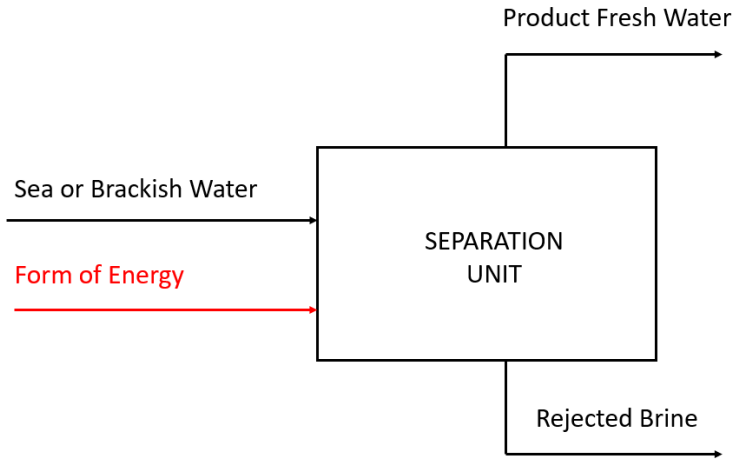

Figure 1.3. Conceptual principle of a desalination process [9].

There are a wide variety of desalination methods, where each works in a different way and has its own characteristics. Figure 1.4. shows the 16 of the most common desalination technologies used.

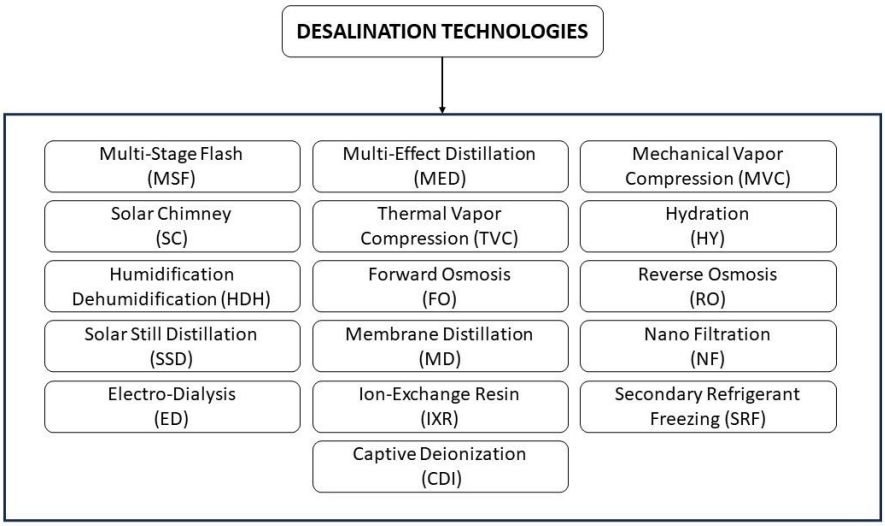

Figure 1.4. Sixteen of the most common desalination technologies [10].

In 2008, 56.5% of the world's desalination plants used reverse osmosis technology and, of the different technologies available, it is still the most widely used [8].

Despite the great advantages of the use of desalination, there are some drawbacks, one of the main ones being the energy consumption required to carry out the separation. In the case of reverse osmosis, for example, high pressures are required, which translates into high energy consumption by the pumps involved in the process. In the last 30 years, significant progress has been made in energy optimization through the development of more efficient membranes. With current reverse osmosis technology, the required energy consumption is 2.0 to 3.0 kWh/m^3. Therefore, the production cost has been reduced below \$ 0.50/m^3 [11].

Another disadvantage is that the rejected brine stream is usually discharged into the ocean. To avoid significantly increasing the salinity of the ocean and damaging marine ecosystems, a relatively small amount of water is desalinated compared to the amount of seawater fed to the process. This concept is known as "recovery".

$$Recovery = \frac{permeate\ volumetric flow\ rate}{fed\ volumetric\ flow\ rate} \times 100 \quad (1.1)$$

Recovery values for a membrane module unit typically range from 8 to 10% for seawater processes and around 15% for brackish water processes [12].

1.3. Desalination industry

In the last few decades, there has been a great growth in the desalination industry field. However, desalination technology was already used more than a thousand years ago. The first people to use this technique were Greek navigators in the 4th century B.C., when seawater was distilled by using furnaces or heaters [13]. The process was carried out in batches and by means of a single separation stage. Energy consumption was high and not very optimized, since the water in the saline solution had to be evaporated. Subsequently, the same steam was condensed to obtain water with a lower salt concentration [9].

The beginning of the desalination industry as such can be considered to be in the middle of the 20th century. The following table shows the most relevant historical developments.

Table 1.2. Historical developments in the desalination field [11].

Year	Achievement
1959	Desalination capability of cellulose acetate film demonstrated by Reid and Breton
1962	Asymmetric cellulose acetate membrane developed by Loeb and Sourirajan
1963	Fist practical spiral-wound module by General Atomics
1967	First commercially successful hollow fiber module by Du Pont
1972	Interfacial composite membrane developed by Cadotte
1975	First commercial interfacial composite installed in a seawater plant by Fluid Systems
1978	First fully aromatic thin film composite (FT-30) by Cadotte
1986	Low-pressure nanofiltration membrane widely available by Fluid Systems
1998	First large hyperfiltration solvent separation plant installed by Grace Davison and Mobil

Nowadays, there are approximately 22,000 desalination plants worldwide [14]. With respect to desalination capacity, the global production is estimated to be close to 80 million cubic meters per day [15]. The three countries with the highest capacity are Saudi Arabia with 17% of global capacity, the United Arab Emirates with 13.4% and the United States with 13.0% [16].

Spain has been one of the pioneering countries in this field; the first desalination plant was installed in 1964 on the island of Lanzarote, producing about 2,500 cubic meters per day [17]. In 2019, there were a total of 765 desalination plants, of which 360

are seawater plants and 405 are brackish water plants (salt concentration from 0.5 to 30 g/L) [18]. Of the total, 99 are large capacity (10,000 to 250,000 m^3/day), 450 are medium capacity (500 to 10,000 m^3/day) and 216 are small capacity (100 to 500 m^3/day). The resulting production capacity is about 5 million cubic meters of desalinated water per day [19]. The main desalination plants in Spain are shown below.

Table 1.3. Desalination plants with the highest capacity in Spain [17] [20].

Ubication [city]	Production capacity [hm^3/year]
Torrevieja, Alicante	80.0
El Atabal, Málaga	76.0
Valdelentisco, Murcia	70.0
Águilas-Guadalentín, Murcia	70.0
Carboneras, Almería	42.0
Campo de Dalias, Almería	30.1
Sagunto, Valencia	25.6
Bahía de Palma, Palma de Mallorca	21.7
De La Marina Baja, Alicante	18.0
Del Bajo Almanzora, Almería	15.0
Oropesa, Castellón	13.5

The resulting capacity of the above desalination plants is 461.9 hm^3/year (about 1.3 million cubic meters per day) however, for practical purposes, the 100% of the capacity of a desalination facility is rarely used.

2. Scope of the project

A series of hypotheses or simplifications have been made when carrying out the project. These are shown below.

1. The energy consumption required to carry out the separation of salt from the feed water will be specifically studied, so the system is considered to be composed only of water and salt with perfect mixing conditions.
2. Other possible stages of the process referred to pre-treatment and post-treatment, such as particle filtration, pH adjustment, disinfection, membrane cleaning and remineralization, among others, will not be taken into consideration.
3. Pressure drop in the equipment (pumps, heater, cooler and membrane module) is not considered.
4. The climatic conditions of the environment do not affect in any way the desalination system by modifying its operating conditions.
5. The thermodynamic properties of the stream fed into the desalination process are kept constant without variations or disturbances.

2.1. Specific objectives

The main objective of the project is to determine the performance offered by the Direct contact membrane distillation technology while minimizing its consumption from an energy point of view. For this purpose, the chemical process simulation software DWSIM is used. There are a series of specific objectives to be taken into account.

1. To understand the working principle of the technology.
2. Obtain and solve the mathematical model that describes the behavior and characteristics of such technology.
3. Validate the results provided by the model via comparison with experimental values.
4. Determine the accuracy of the model.
5. To implement the equations in the DWSIM simulation environment.
6. Perform sensitivity analysis and minimize energy optimization using the software.
7. Obtain results for a possible pilot plant working with such technology.

3. Role in the company

Eurecat is a technology center in Catalonia where national or European projects are carried out covering a wide range of industry sectors, including the chemical, food, energy, finance, health and many others. The main objective of Eurecat is to provide technological solutions to promote the competitiveness of companies and the welfare of society.

In addition, there are four main areas of knowledge in which the professionals at the center are divided. These are the industrial area, the digital area, the biotechnological area and the sustainability area. In this last one is where this project is carried out, specifically in the technological unit WAS (Water, Air and Soil), where R+D+I (research, development and innovation) projects are carried out to improve the management of water, air and soil.

At the beginning of the internship experience, since it was an R+D+I type project, it was essential to carry out an exhaustive state of the art, in this case, on desalination technologies, on the basis of which the study was to be carried out. In the bibliographic search, books related to separation technologies and unitary operations were consulted, as well as scientific articles in different databases such as *Web of science* or *Scopus*.

With regard to desalination technologies, an attempt was made to obtain a mathematical model that defines the behavior of a membrane distillation and reverse osmosis unit. Membrane distillation technology is divided into different variants, including Direct contact membrane distillation (DCMD), Air gap membrane distillation (AGMD) and Vacuum membrane distillation (VMD). Of the three variants mentioned, only a satisfactory mathematical model was obtained for DCMD. On the other hand, in the case of reverse osmosis (RO), a mathematical model could also be obtained.

The next stage carried out consists of the implementation of the mathematical models in a simulation environment. For that the chemical process simulation software DWSIM is used. The simulator does not have the mathematical procedure to calculate a DCMD or RO unit, so the equations of the mathematical models previously established for the two technologies had to be introduced. In this case the Python programming language is required when introducing the equations. Subsequently, the Newton Raphson method for solving systems of nonlinear equations has been implemented in the code, which allows the defined equations to be solved through an iterative process. Also, the relationship of the properties of the feed and output streams connected to the code unit is established. Once the simulator is working correctly with

the two desalination technologies DCMD and RO, different sensitivity analyses are carried out for the subsequent energy optimization of the two technologies.

On a weekly basis, Eurecat has been following the development of this study through telematic and face-to-face meetings, providing feedback on the progress made at each meeting.

4. Direct contact membrane distillation

Membrane distillation (MD) is one of the emerging technologies in the field of water desalination. About 25% of the desalination processes are currently carried out using this method [21]. It combines conventional distillation with membrane technology.

The transport across the membrane is thermally driven, as a result of the temperature difference between the two sides of the membrane. The temperature difference results in a vapor pressure difference which is the driving force of the system. Due to the hydrophobic membranes used, the water used as solvent manages to pass through the membrane by means of a phase change. However, the non-volatile solute (salt in this case) does not easily pass through the membrane. Thus, the solvent can be extracted in a high concentration.

It is important to mention that within membrane distillation there are different types of variants depending on the requirements of a process or applications. The most common are: Direct contact membrane distillation (DCMD), Air gap membrane distillation (AGMD), Vacuum membrane distillation (VMD) and Sweeping gas membrane distillation (SGMD).

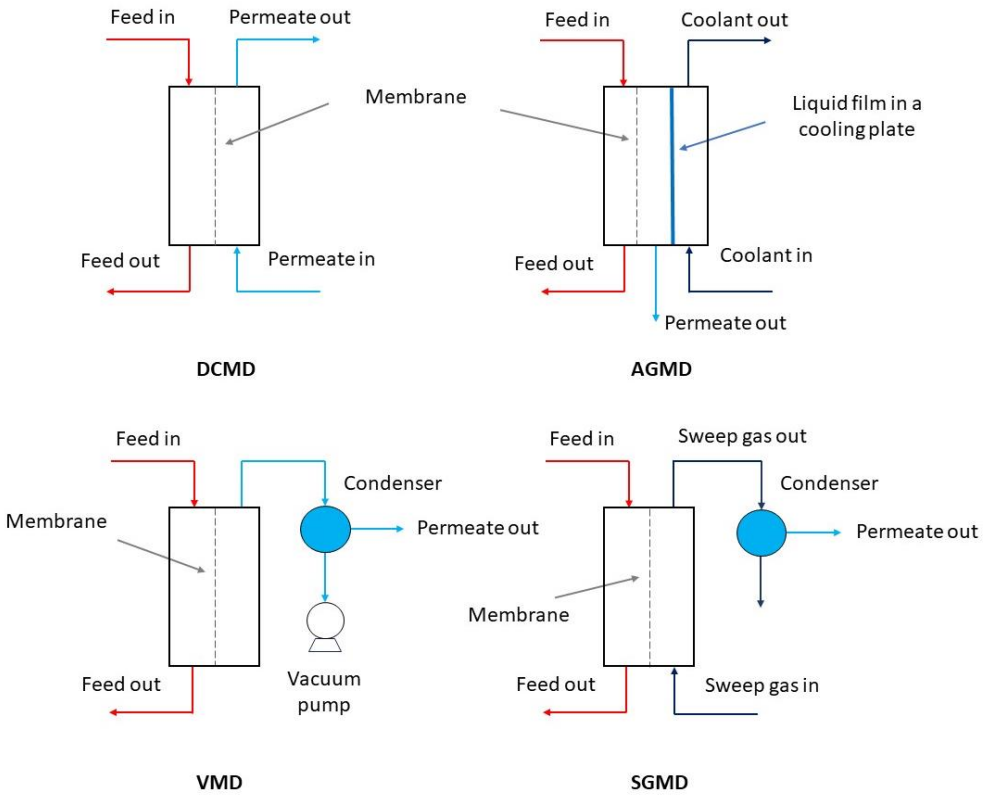

Figure 4.1. Different membrane configurations for each of the DCMD variants [22].

DCMD: The permeate stream is in direct contact with the membrane in the same way as the feed stream. By means of a cooler, the temperature of the permeate stream is kept constant and recirculated. A part of the permeate stream is separated as a product, resulting in a water flow with low solute concentration.

AGMD: On the permeate side of the membrane there is an air gap which is in contact with a cooling plate. The cooling plate is cooled by means of a refrigerant, resulting in condensation of the vapor passing through the membrane. Subsequently, the condensate is obtained as a distillate product.

VMD: Vacuum is created by a pump on the permeate side of the membrane. The vapors that pass through the membrane condense out of the membrane, allowing the product stream to be obtained.

SGMD: In this case, a gas is used to strip off the vapor that pass through the membrane. Subsequently, the gas stream is cooled, condensing the vapors that have passed through the membrane. Finally, a stream containing only the distilled product is obtained.

Direct contact membrane distillation is the most used in seawater desalination due to its main advantages over the other variants. These include low capital cost, simplicity and relatively high permeate fluxes. However, it also has its drawbacks, the most significant of which is the high conduction losses across the membrane [21].

4.1. DCMD working principle

A Direct contact membrane distillation system consists of a membrane module, but also of a heat exchanger and pumping systems. The following is a typical schematic of an experimental Direct contact membrane distillation system used in a laboratory.

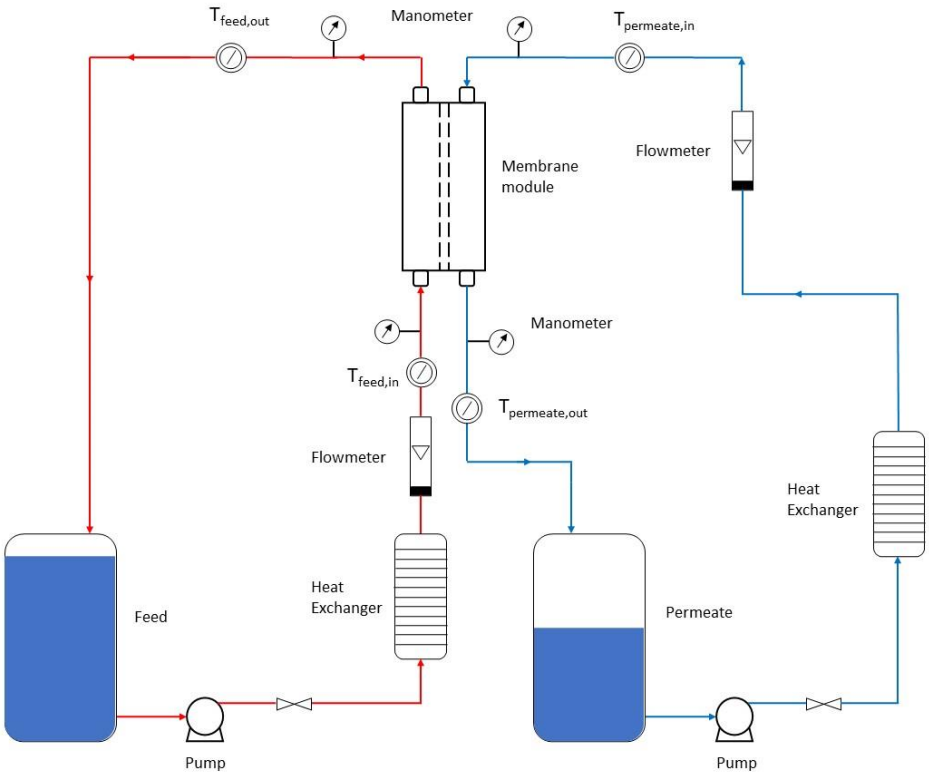

Figure 4.2. Schematic of an experimental DCMD laboratory system [22].

As can be seen in the picture above, the process starts from a solution of water with a certain salt concentration, for example, it could be brackish water or seawater. It is then pumped through a heater, where the salty stream reaches a temperature slightly above room temperature (about 30ºC) or up to 90ºC [22]. Provided that it is in liquid phase. The hot solution is kept in direct contact with the feed side of the membrane. Where the fluid moves in the direction tangential to the membrane surface. A fraction of this same stream passes through the membrane known as permeate. On the other hand, most of it does not pass through and is recirculated back to the beginning of the process that is usually a tank (if it's a non-stationary system as in this example).

The hydrophobic nature of the membrane prevents the liquid phase solution from entering the pores due to surface tension. In this way, liquid-vapor interfaces are formed in the pores on the membrane surface. The difference in temperature on the two sides of the membrane gives rise to a difference in vapor pressures. As pure water is a volatile component, its molecules evaporate at the liquid-vapor interfaces generated on the hot side, thus crossing the membrane in vapor phase from the hot to the cold side. On the cold one, vapors condense as they reach the vapor-liquid interfaces.

The permeate stream that does pass through the membrane, has a significantly low salt concentration. This stream goes to a secondary tank, next is pumped and cooled by a cooler. Finally, it passes back through the membrane by creating a temperature difference on both sides of the membrane. The temperature of the permeate stream can vary from room temperature (about 25°C to temperatures of 5°C).

It should be noted that the experimental scheme shown above does not operate in steady state, since the system is closed. In this case the salt concentration in the feed tank will increase with time as well as its volume will be reduced. On the other hand, the permeate tank with low salt concentration will fill up.

In the following image, the different conditions on the two sides of the membrane can be seen in detail.

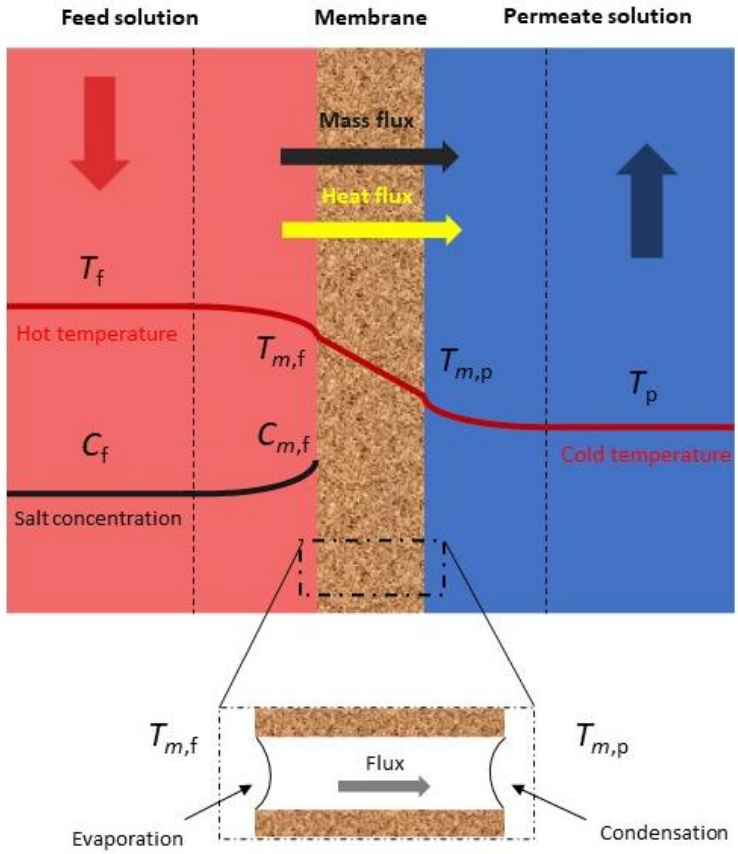

Figure 4.3. Schematic of the feed and permeate solutions in direct contact with the membrane module in DCMD technology [23].

As the solution on the feed side approaches the membrane surface, the salt concentration increases until it peaks at the surface itself. This is because near the

membrane wall, the water passes to the other side thus accumulating the salt. This phenomenon is known as concentration polarization.

In this technology, the water flux across the membrane depends directly on the temperature difference on the two sides of the membrane leading to a vapor pressure difference. Therefore, the greater difference it is on the two membrane sides, the greater the flux of water with low salt concentration. However, a greater temperature difference is equivalent to a higher operating energy cost.

4.2. DCMD mathematical model

In order to subsequently simulate the behavior of a DCMD unit through software, an exhaustive literature search has been carried out. Different mathematical models from scientific articles have been studied. Finally, it has been decided to implement the model proposed by the paper: "*Experimental and theoretical investigations on water desalination using direct contact membrane distillation*" [24]. Most of the energy and mass balance equations come from the article mentioned above.

In the mathematical model, only the membrane module unit itself is considered. The recycles and other equipment that allow the membrane unit to operate are not taken into account in the equations below, they are subsequently calculated by the simulator.

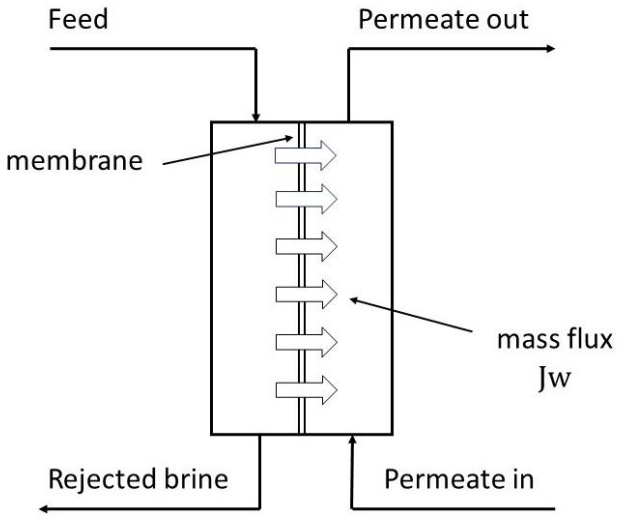

Figure 4.4. Schematic of the membrane module of a DCMD system.

As can be seen, only four streams define the membrane module. In total there are two inputs and two outputs.

4.2.1. Energy balance

In DCMD the energy balance of the module is divided into three stages, which are:

1. Energy transfer from the feed solution to the hot wall of the membrane.
2. Energy transfer in the membrane itself.
3. Energy transfer from the cold membrane wall to the permeate solution.

Each of the above-mentioned stages has a significant influence on the performance of a direct contact membrane distillation unit. In the following, each one is explained.

1st Stage. The energy transfer between the feed solution and the hot membrane wall is given by Newton's law of cooling. In order to calculate the convection coefficient h, it is necessary to use a series of equations where the dimensionless Reynolds, Prandtl and Nusselt numbers that depend on the properties of the solution stream flowing in contact with the membrane are found.

$$Q_f = h_f \times (T_f - T_{m,f}) \tag{4.1}$$

2n Stage. In the case of energy transfer across the membrane. A portion is used to evaporate the water at the liquid-vapor interface from the pores on the hot side, leading to a phase change. However, the other part of the energy reaching the membrane is transferred across the membrane by the phenomenon of conduction.

$$Q_m = Q_c + Q_v \tag{4.2}$$

$$Q_v = J_w \times \Delta h_v \tag{4.3}$$

$$Q_c = \frac{k_m}{\delta_m} \times \left(T_{m,f} - T_{m,p}\right) \tag{4.4}$$

The vaporization enthalpy at the membrane wall can be estimated from the following correlation:

$$\Delta h_v = \left(1.7535 \times T_{m,f}\right) + 2024.3 \tag{4.5}$$

It should be noted that the above expression is valid for the range 273 to 373 K [25]. In addition, the resulting units are kJ/kg.

The conductivity of the membrane depends on the conductivity of the vapor that crosses it, as well as the conductivity of the polymer and the porosity. According to the bibliography [25], there are three different methods that can be used to predict the value of the thermal conductivity of the membrane.

The isostress or series method:

$$k_m = \left(\left(\frac{\varepsilon}{k_{vap}}\right) + \left(\frac{1-\varepsilon}{k_{pol}}\right)\right)^{-1} \tag{4.6}$$

The isostrain or parallel method:

$$k_m = \varepsilon \times k_{vap} + (1-\varepsilon) \times k_{pol} \tag{4.7}$$

The flux law method:

$$k_m = k_{vap} \times \left[\frac{1 + (1-\varepsilon) \times \beta_{s-g}}{1 - (1-\varepsilon) \times \beta_{s-g}}\right] \tag{4.8}$$

$$\beta_{s-g} = \frac{k_{pol}/k_{vap} - 1}{k_{pol}/k_{vap} + 2} \tag{4.9}$$

In order to estimate the membrane conductivity, the isostress method is followed in the same way as in the article on which this same model is based.

3rd Stage. Finally, the energy present on the cold side of the membrane is transferred to the permeate stream by convention. As in the case of the first stage, the higher the value of the convection coefficient, the greater the energy transfer.

$$Q_p = h_p \times (T_p - T_{m,p}) \tag{4.10}$$

In each of the three stages, there is an opposition or resistance to the passage of energy. The following image shows this concept more clearly.

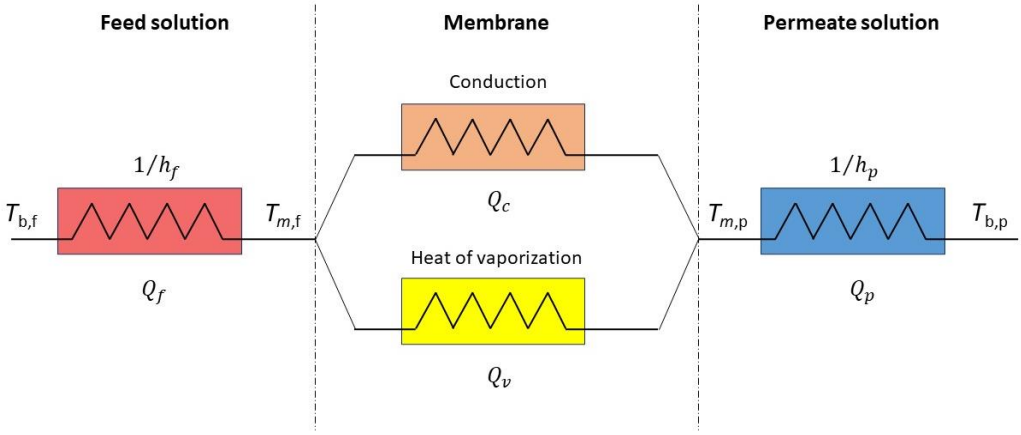

Figure 4.5. Illustration of energy transfer resistances in the 3 stages of DCMD [22].

The convection coefficients on both sides of the membrane depend on the Nusselt number, thermal conductivity and hydraulic diameter.

$$h = \frac{Nu \times k}{D_h} \tag{4.11}$$

The hydraulic diameter is defined from the fluid flow area and the wetted perimeter.

$$D_h = \frac{4 \times A_c}{P} \tag{4.12}$$

To calculate the Nusselt number, the values of the dimensionless numbers Reynolds and Prandtl must first be calculated.

$$Re = \frac{u \times D_h}{v} = \frac{\rho \times u \times D_h}{\mu} \tag{4.13}$$

$$Pr = \frac{\mu \times C_p}{k} \tag{4.14}$$

The fluid velocity u can be calculated from the volumetric flowrate (for both feed and permeate streams divided by their respective passage areas).

$$u = \frac{\dot{v}}{A} \tag{4.15}$$

The Nusselt is estimated from different correlations depending on the flow regime. In the case of laminar flow (Re<2300), the expression used is as follows:

$$Nu = 1.86 \times \left(Re \times Pr \times \frac{D_h}{L}\right)^{1/3} \tag{4.16}$$

Where L corresponds to the channel length from which the fluid is in direct contact with the membrane.

In the case of a transitional or turbulent regime (Re>2300), the Nusselt value is estimated from the following equations, where the exponent of the Prandtl number is different depending on if the stream is heating or cooling [26].

$$Nu_f = 0.027 \times Re^{0.8} \times Pr^{0.4} \times \left(\frac{\mu_f}{\mu_{m,f}}\right)^{0.14} \tag{4.17}$$

$$Nu_p = 0.027 \times Re^{0.8} \times Pr^{0.3} \times \left(\frac{\mu_p}{\mu_{m,p}}\right)^{0.14} \tag{4.18}$$

By performing the global energy balance in the membrane unit, the overall heat transfer can be determined. However, this equation is not necessary for the resolution of the mathematical model.

$$U = \left(\frac{1}{h_f} + \frac{1}{\left(\frac{k_m}{\delta_m}\right) + \left(\frac{J_w \times \Delta H_v}{T_{m,f} - T_{m,p}}\right)} + \frac{1}{h_p}\right)^{-1} \tag{4.19}$$

4.2.2. Mass balance

As mentioned above, the flux of water vapor through the membrane depends directly on the difference of the vapor pressures on the two sides of the membrane, but it also depends on parameter named equivalent diffusion coefficient D_e. It corresponds to the diffusion coefficient of water vapors through the membrane pores.

The value of the D_e coefficient is determined from the contribution of two other diffusion coefficients, the molecular diffusion coefficient D_m and the Knudsen diffusion coefficient D_k. Depending on which of the two types of diffusion is predominant, the flux through the membrane will be strongly affected [23] [24] [27].

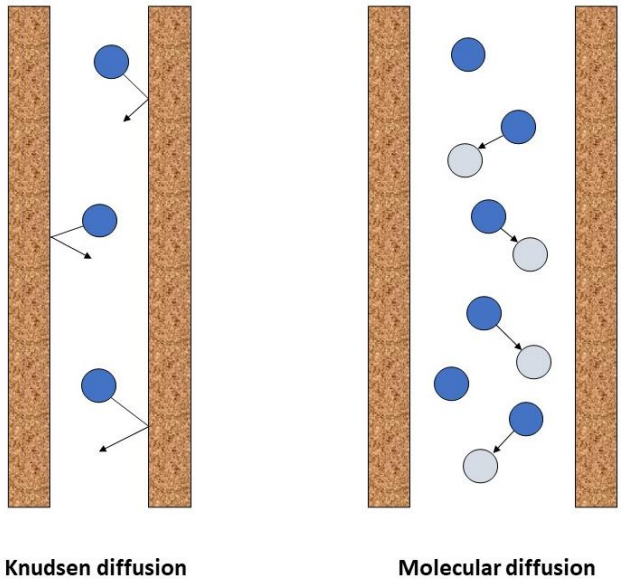

Figure 4.6. Mechanisms of mass transport through a pore in DCMD technology [22].

In Knudsen diffusion, collisions between molecules and the pore wall are predominant. However, in molecular diffusion collisions between molecules within the pore predominate.

The value of the Knudsen number determines the contribution of the Knudsen and molecular diffusion to the equivalent diffusion coefficient. Which depends on the mean free path across the membrane divided by the pore diameter [21] [22].

$$Kn = \frac{\lambda}{d_{pore}} \tag{4.20}$$

The mean free path depends on Boltzmann's constant ($1.38065 \times 10^{-23}\ in\ J/K$), the average membrane temperature, the pore pressure and the collision diameter of the water vapor molecules ($2.641 \times 10^{-10}\ in\ m$).

$$\lambda = \frac{k_B \times T_m}{\sqrt{2 \times \pi} \times P_{pore} \times {\sigma_v}^2} \tag{4.21}$$

In the case that $Kn > 10$, the Knudsen diffusion predominates. However, if $Kn < 0.01$, the molecular diffusion sets the behavior of the mass transport. Finally, for the case that $0.01 < Kn < 10$, there is a contribution of both Knudsen and molecular diffusion. As will be seen below, a coefficient "α" is used in the model which adjusts the relationship of the two types of diffusion by means of the experimental results.

First, the vapor pressures of water are calculated from the wall temperatures on the two sides of the membrane using Antonie's equation.

$$p_{m,f}^{0} = exp\left(23.1964 - \frac{3816.44}{T_{m,f} - 46.13}\right) \quad (4.22)$$

$$p_{m,p}^{0} = exp\left(23.1964 - \frac{3816.44}{T_{m,p} - 46.13}\right) \quad (4.23)$$

Due to the presence of dissolved salt in the water on the feed side, an activity coefficient is used to correct the vapor pressure value. Where its value depends on the salt mole fraction.

$$a_{w,f} = 1 - 0.5 \times x_{Nacl,f} - 10 \times \left(x_{Nacl,f}\right)^2 \quad (4.24)$$

$$p_{m,f,c}^{0} = p_{m,f}^{0} \times \left(1 - x_{Nacl,f}\right) \times a_{w,f} \quad (4.25)$$

For the estimation of membrane tortuosity, there are two commonly used expressions for polymeric membranes. The difference between the two groups can be attributed to the manufacturing methods and the resulting pore morphologies [28].

Loose packed spheres:

$$\tau = \frac{1}{\varepsilon} \quad (4.26)$$

Interstices between closed packed spheres:

$$\tau = \frac{(2 - \varepsilon)^2}{\varepsilon} \quad (4.27)$$

The loose packed spheres model is the one followed in this case since is the one used in the article followed.

The membrane temperature is estimated as the average of the temperatures on both sides on the wall.

$$T_m = \frac{T_{m,f} + T_{m,p}}{2} \quad (4.28)$$

The diffusivity of the water vapors produced through the static air inside the membrane is then calculated.

$$PD_{w,a} = 1.895 \times 10^{-5} \times T_m^{2.072} \tag{4.29}$$

Subsequently, it is required to determine the total pressure inside the pores, the partial pressure of water vapors inside the pores and the partial pressure of air inside the membrane pores.

$$P_{pore} = \frac{p_f + p_p}{2} \tag{4.30}$$

$$P_{w,v,p} = exp\left(23.1964 - \frac{3816.44}{T_m - 46.13}\right) \tag{4.31}$$

$$P_{air,pore} = P_{pore} - P_{w,v,p} \tag{4.32}$$

The molecular and Knudsen diffusions are estimated from the following expressions respectively:

$$D_m = \left(\frac{R_{gas} \times T_m \times \delta_m \times \tau \times P_{air,pore}}{MW_{H2O} \times \varepsilon \times PD_{w,a}}\right)^{-1} \tag{4.33}$$

$$D_k = \left(\left(\frac{3 \times \delta_m \times \tau}{2 \times \varepsilon \times d_{pore}}\right) \times \left(\frac{\pi \times R_{gas} \times T_m}{8 \times MW_{H2O}}\right)^{0.5}\right)^{-1} \tag{4.34}$$

The contribution of previous diffusions to the equivalent diffusion coefficient is given by:

$$D_e = \left(\left(\frac{\alpha}{D_k}\right) + \left(\frac{1-\alpha}{D_m}\right)\right)^{-1} \tag{4.35}$$

As can be seen, for a value of the parameter "α" close to 0, molecular diffusion dominates mass transport along the membrane. However, for alpha values close to 1, Knudsen diffusion dominates.

The mass flux through the membrane unit is given by the difference between vapor pressures multiplied by the equivalent diffusion coefficient.

$$J_w = D_e \times \left(p^0_{m,f,c} - p^0_{m,p}\right) \tag{4.36}$$

4.3. DCMD iterative calculation procedure

To calculate the energy balance, the temperatures of the two membrane walls have to be calculated from the following equations.

$$T_{m,f} = \frac{k_m \times \left(T_p + \frac{h_f}{h_p} \times T_f\right) + \delta_m \times \left(h_f \times T_f - J_w \times \Delta h_v\right)}{k_m + h_f \times \left(\delta_m + \frac{k_m}{h_p}\right)} \tag{4.37}$$

$$T_{m,p} = \frac{k_m \times \left(T_f + \frac{h_p}{h_f} \times T_p\right) + \delta_m \times \left(h_p \times T_p + J_w \times \Delta h_v\right)}{k_m + h_p \times \left(\delta_m + \frac{k_m}{h_f}\right)} \tag{4.38}$$

Where $T_{m,f}$ is the temperature at the feed side and $T_{m,p}$ at the permeate one. Both temperatures depend on several parameters, including the water vapor flux across the membrane J_w. However, the vapor flux is obtained as a result of the mass balance, and it also depends on the value of the temperatures on the two sides of the membrane.

To solve the system an iterative process has to be carried out. Where initially it will be assumed that the values of the membrane wall temperatures are close to the temperatures of the feed and permeate streams. Next, the mass balance is calculated to determine the water vapor flux through the membrane. Knowing the flow rates, the convection coefficients on both sides of the membrane are calculated, considering also the pipe sizing in both cases. Finally, the new values of the temperatures on the two membrane walls are calculated.

This iterative process has to be repeated until the values of the temperatures on both sides of the membrane obtained are very close or equal to those of the previous iteration.

In the following image, it is easier to visualize the iterative process carried out.

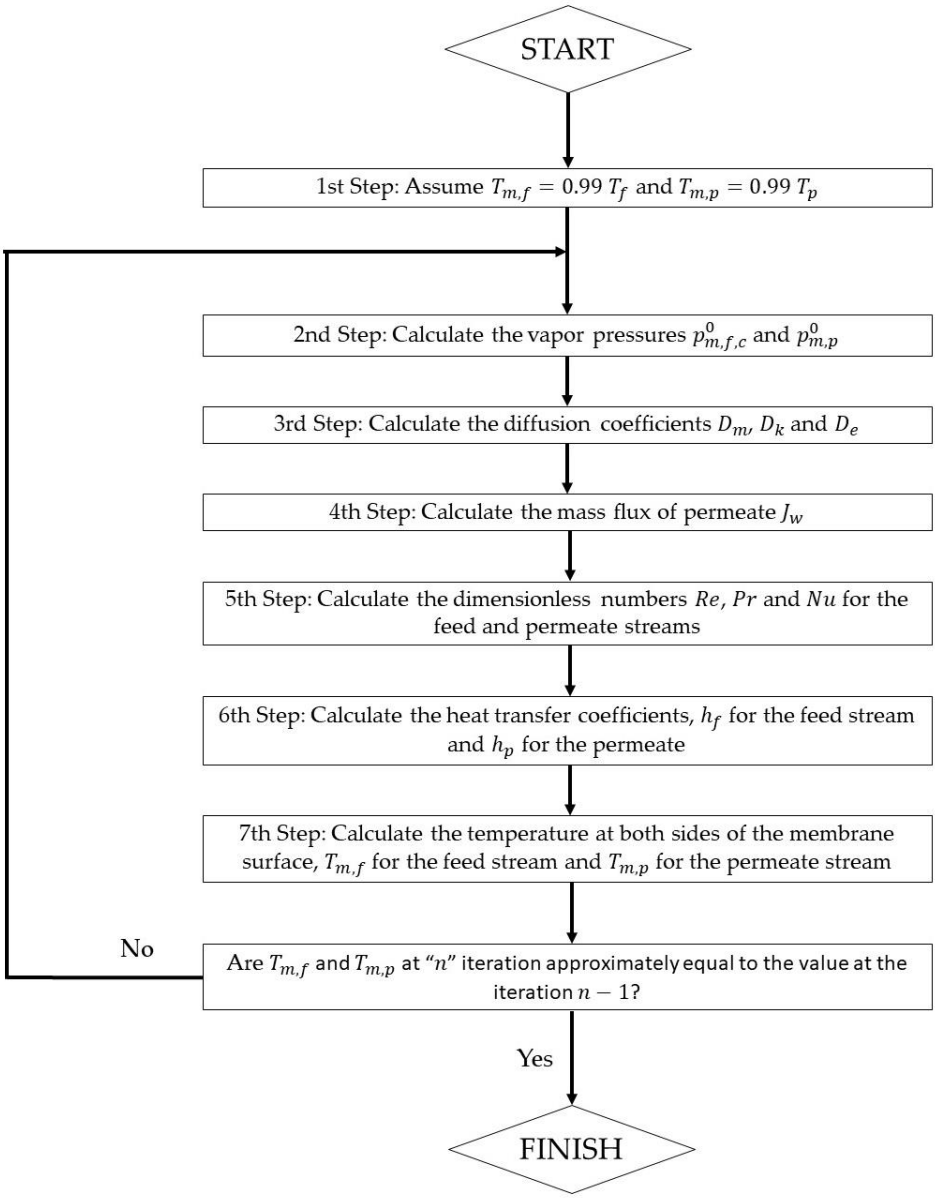

Figure 4.7. Iteration procedure for the calculation of temperatures on both sides of the membrane surface on a DCMD membrane module.

4.4. DCMD model validation

Once the model of the DCMD unit has been determined, a comparison of the results obtained from the mathematical model with the experimental results provided in the article [24] is carried out.

In the resolution of the energy balance, the values of different thermodynamic properties, such as viscosity, thermal conductivity, heat capacity and density are required for the calculation of the convection coefficients on both sides of the membrane, in addition, the value of the conductivity of the water vapor passing through it is also required.

First, the model was derived by considering the thermodynamic properties from the table of pure properties of water, namely Table A-9 in Appendix 1 of the book "*Heat and mass transfer fundamentals & applications*" [29]. The program used for this purpose was Microsoft Excel®, which allows the model to be solved by automatically interpolating the values of the properties in the table.

It is important to note that, considering the properties of pure water, the results obtained are valid for low salt concentrations. The experimental results provided in the article have been carried out at a concentration of 2 g/L, so this first resolution is a good approximation.

Subsequently, the mathematical model was also solved in another way. This time, instead of interpolating a table of thermodynamic properties, correlations were used [9] [30]. The use of correlations allows estimating the properties as a function of temperature but also salinity. In this way, the resolution of the model provides more accurate results for higher salt concentrations. The Microsoft Excel® program was also used for this purpose.

The only difference in the method of resolution is that in the first case, when interpolating the properties, the system of equations has two variables to iterate which correspond to the temperatures on the two membrane walls. In the second case, since salinity is a function of density, it is required to use a density value to calculate salinity and then recalculate that density. Therefore, in the use of correlations there are actually a total of four variables, the temperatures on the two walls and the density of the feed and permeate streams. The values of the pure water properties as well as the correlations used are shown in Appendix A.

In order to compare the results obtained by the mathematical model (using the two methodologies) with the experimental results, the same parameter values and operating conditions are used as in the article. In the following table the used values can be seen

Table 4.1. Experimental working conditions and parameter values according to the article followed [22].

Parameter	Value
Feed salt concentration	2 g/L
Feed volumetric flowrate	4.60 L/min
Permeate volumetric flowrate	3.65 L/min
Feed stream pressure	2.4 bar
Porosity	0.8
Membrane thickness	154 μm
Pore diameter	379 nm
Membrane area	0.06192 m^2
Nº of channels	3
Channel length	66 mm
Channel width	24 mm
Channel depth	5 mm

The membrane used in the experimental results corresponds to PTFE-SF17386, made from polytetrafluoroethylene. However, not all the information required to carry out the calculations is available, so a total of 3 different assumptions have been made.

4.4.1. Assumptions

1. In the article followed [24], no information is provided on the thermal conductivity of the membrane polymer. However, by searching for the same type of membrane, its conductivity is expected to be close to 0.25 W/(m·K) [31]. Therefore, this conductivity value is the one used in the calculations.

2. Likewise, the pressure of the permeate stream is not specified, in this case, the same pressure as in the feed stream, about 2.4 bar, is considered.

3. The value of the parameter "α" is also unknown, so initially different values between 0 and 1 have been tested for specific conditions. The values of the flux through the membrane obtained by solving the mathematical model when the temperature of the permeate stream is 10ºC are shown below.

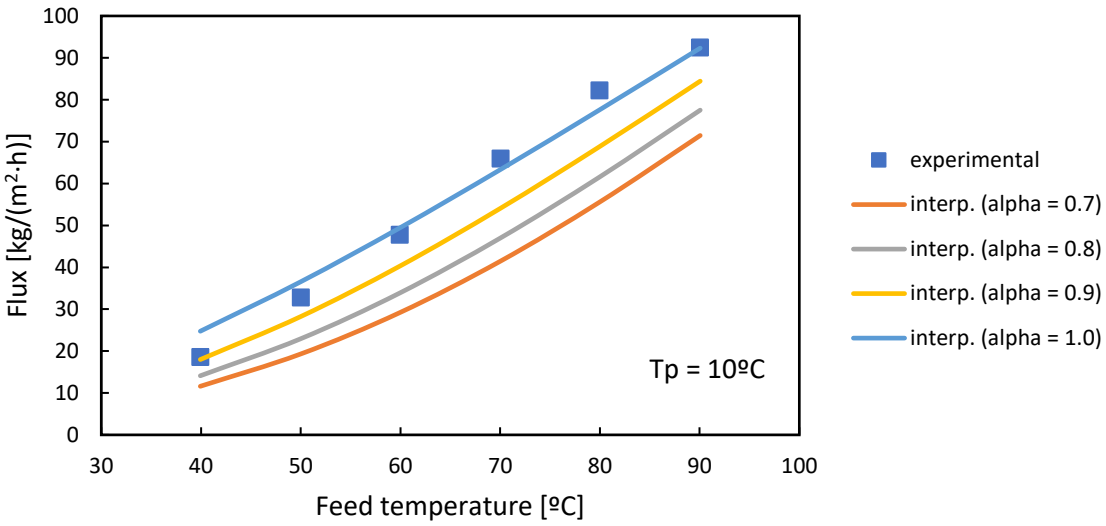

Figure 4.8. Fluxes through the membrane as a function of feed temperature for a permeate temperature of 10ºC, considering different Knudsen and molecular diffusion contributions.

On the one hand, it can be observed that the results obtained agree closely with those of the article for alpha parameter "α" values of 1, where the Knudsen diffusion parameter is the only one considered in the transfer of mass through the membrane pores. On the other hand, the contribution of molecular diffusion significantly affects the results obtained by decreasing the fluxes across the membrane, moving them away from the experimental results.

By means of the calculation of the free path "λ" and the Knudsen parameter "Kn" it is verified whether it is really considered one type of diffusion or both Knudsen and molecular diffusions. For the range of feed temperatures considered in the figure above from 40 to 90°C, the Knudsen parameter value varies from 0.15 to 0.16. Therefore, how $0.01 < Kn < 10$ technically inside the membrane should be a contribution of molecular and Knudsen diffusion coefficients.

Finally, in the resolution of the model it is assumed that the value of the alpha parameter is 1 considering only Knudsen diffusion, because of the close results obtained with the experimental ones. This simplification means that molecular diffusion is not considered. Therefore, the vapor flux through the membrane does not depend on the operating pressure according to the mass balance.

4.4.2. Validation with experimental results

Once the assumptions required to determine all the parameters of the mathematical model have been made, it is proceeded to compare the results obtained by the model with the experimental results [24].

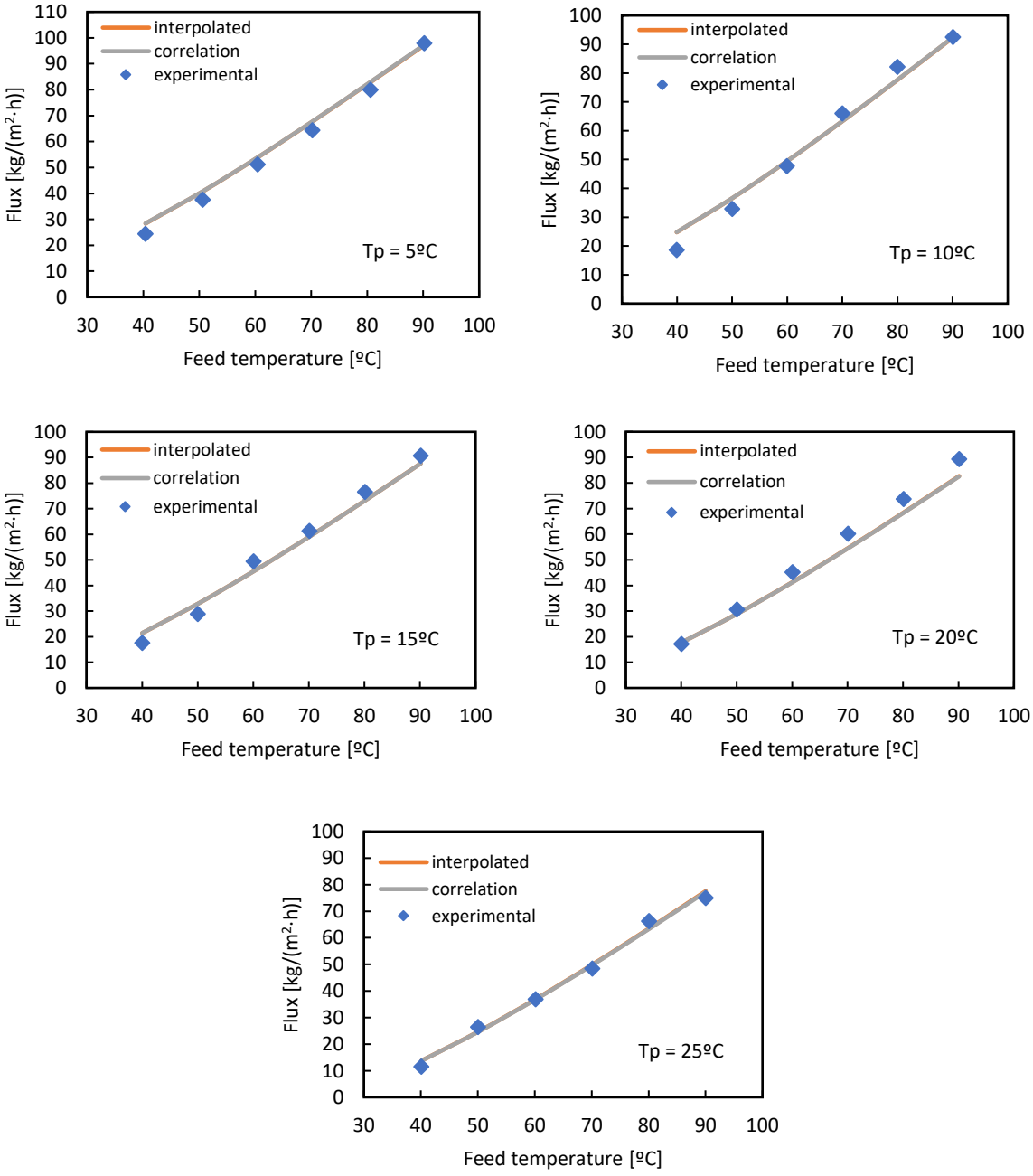

Figure 4.9. Fluxes through the membrane (experimental, interpolated and by means of using correlations) as a function of feed temperature for permeate temperatures of 5, 10, 15, 20 and 25ºC.

As it can be seen, the results obtained by the different ways of estimating the thermodynamic properties (interpolating or using correlations) are practically identical. In fact, the lines overlap so that they are indistinguishable to the naked eye. In addition, the results obtained with the model are in good agreement with those provided in the paper. A lower temperature of the permeate stream implies, as expected, a higher flux through the membrane for the same feed temperature value.

If, instead of varying the permeate temperature for different cases, the feed temperature is varied, the results obtained are similar.

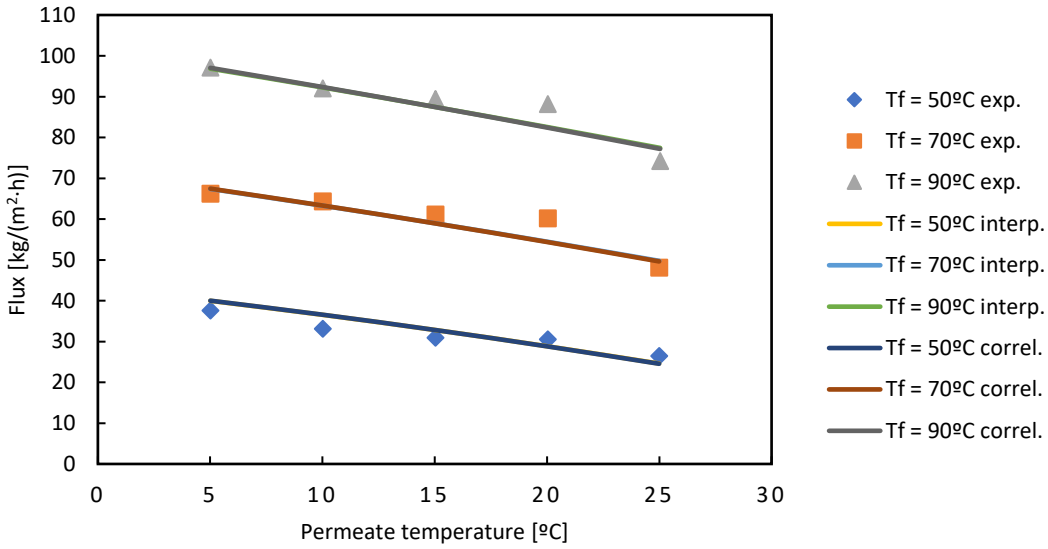

Figure 4.10. Fluxes through the membrane as a function of permeate temperature for different feed temperatures.

For the same permeate stream temperature, the higher the feed flow temperature, the higher is the flow rate across the membrane. Strictly, the correlations used are adequate for temperatures above 10°C, however, for the sake of comparison with the experimental results, an exception has been made in this case. The results obtained numerically for each of the above figures are shown in Appendix B.

As mentioned above, the estimation of thermodynamic properties from pure water properties is a good approximation for low concentrations. The same procedure is then repeated but, in the feed, a concentration of 38 g/L (the concentration of the Mediterranean Sea [8]) is considered instead of 2 g/L. The values of the other parameters are the same as shown in the table above.

The following graph shows the results obtained for permeate temperatures of 10, 15, 20 and 25ºC.

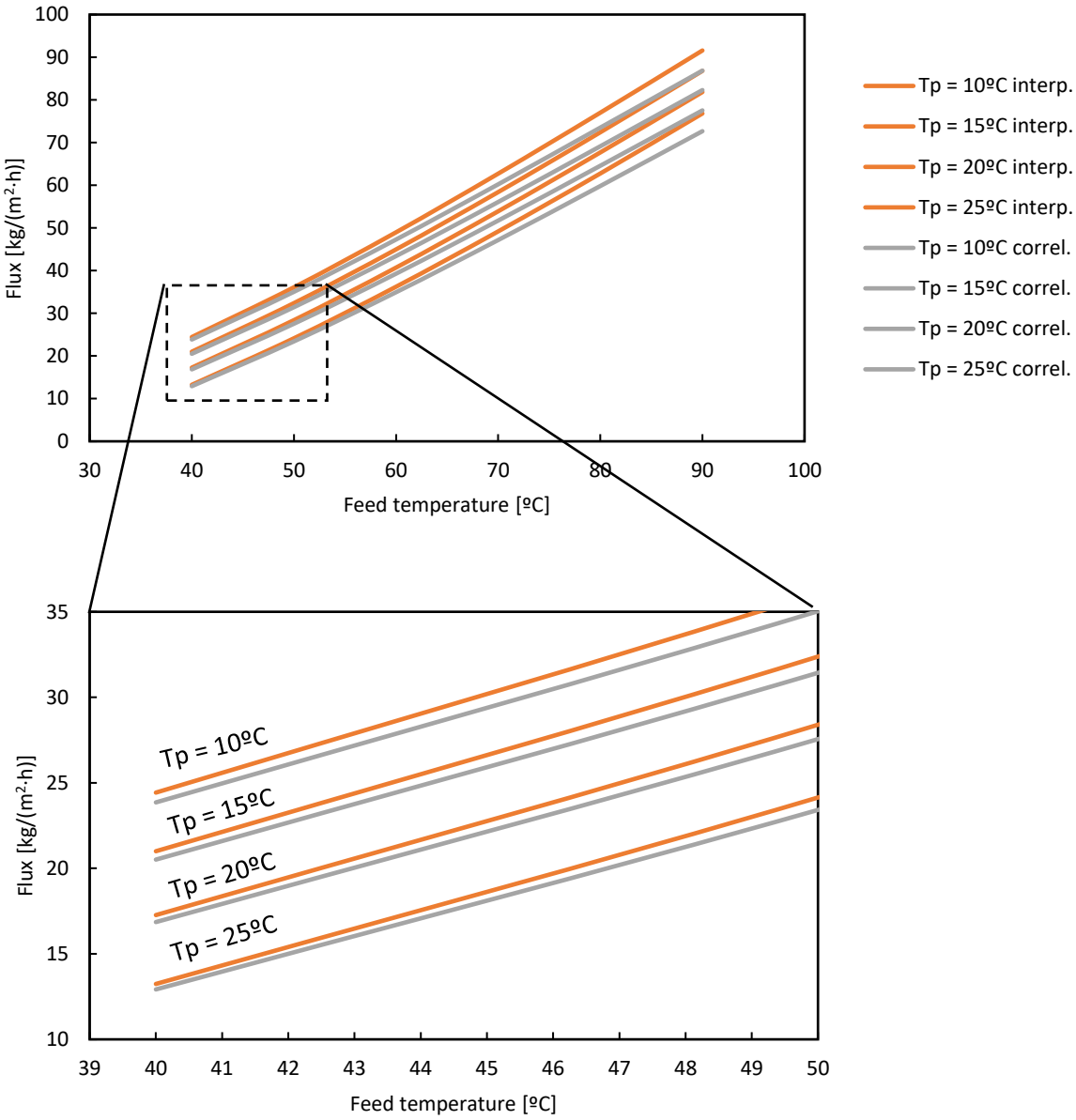

Figure 4.11. Fluxes through the membrane as a function of feed temperature for different permeate temperatures, for a salt feed concentration of 38 g/L.

As it can be seen in the figures above, for the 38 g/L concentration the results obtained by the two methodologies are more different. The fluxes through the membrane vary more markedly depending on how the thermodynamic properties are determined. Moreover, at higher temperature difference between the feed and permeate streams, the presence of salt substantially influences the values of the thermodynamic properties used in the mathematical model. Therefore, as expected, the approach of using the pure water properties is adequate for low salt concentrations as well as for small temperature differences between the two streams.

4.4.3. Accuracy of the mathematical model

The results obtained are satisfactory, however, in order to quantify the accuracy offered by the model developed with respect to the experimental values, the error of the model is determined. Of the two procedures used to determine the thermodynamic properties, error is calculated in the case where empirical correlations are used. However, for a concentration of 2 g/L as seen above, either of the two methods is valid.

The following equations are used to determinate the average, standard deviation, mean deviation and the total error of a sample of values.

$$X_m = \frac{1}{n}\sum_{i=1}^{n} X_i \tag{4.39}$$

$$\sigma^2 = \frac{1}{n-1}\sum_{i=1}^{n} (\Delta X_i)^2 \tag{4.40}$$

$$\sigma_m = \frac{\sigma}{\sqrt{n}} \tag{4.41}$$

$$\varepsilon_t = (\sigma_m + \varepsilon_{SI}) \tag{4.42}$$

The systematic error ε_{SI} associated with the measurement of the flow rate through the membrane is unknown, so as an approximation, it is not considered in the calculation of the model error. The error associated with each of the sample values represented in the figures 4.9. and 4.10. is shown below.

Table 4.2. Error values committed by the mathematical model for the different sample values with respect to the experimental results.

Parameter	Error %
T_p = 5ºC	6.6 ± 2
T_p = 10ºC	9.7 ± 5
T_p = 15ºC	9.1 ± 3
T_p = 20ºC	7.0 ± 0.9
T_p = 25ºC	6.0 ± 3
T_f = 50ºC	7.2 ± 0.8
T_f = 70ºC	4.0 ± 2
T_f = 90ºC	2.7 ± 3

For elevated temperatures in both the feed and permeate streams, the error seems to decrease, with the exception of the sample values carried out at a T_p of 5ºC. Furthermore, in most of the results obtained there is a significant uncertainty, this is due to the large difference of the results provided by the model with some of the experimental values.

The comparison of the values calculated by the mathematical model with the experimental results is shown below.

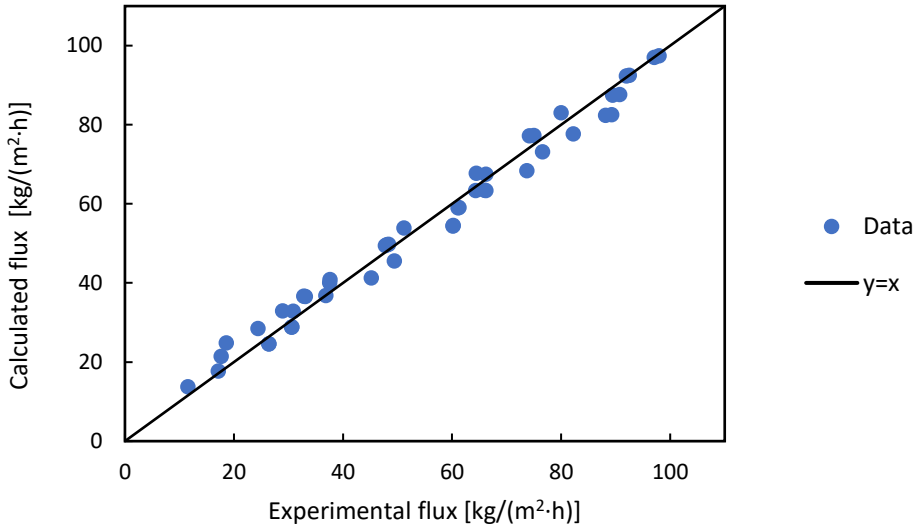

Figure 4.12. Model prediction results against the experimental values of permeate flux (45 dots).

If all the value samples are considered at the same time, the total error of the model from the 45 experimental values studied corresponds to 6.7 ± 0.9%. Appendix B contains the calculations performed for the determination of the model error in more detail.

5. Implementation in DWSIM

Using the chemical process simulation program DWSIM, the Direct contact membrane distillation technology is modeled.

The great advantage of using software is that it allows the mathematical model to be calculated quickly and automatically, thus facilitating the study of the behavior of the model itself as a function of the different parameters that make it up.

Sensitivity analyses are very useful when optimizing chemical processes. In addition, DWSIM has a thermodynamic database for the calculation of desalination systems called: IAPWS-08 Seawater.

However, DWSIM does not have the mathematical equations that allow the calculation of the membrane module in which the separation of water and salt takes place implemented by default. Therefore, a "User model" called "Python Script" has to be created in which the equations of the system are defined manually using the Python programming language.

The multivariable Newton-Raphson method is used to solve the non-linear equations of the model in the developed code. This allows the temperatures on both sides of the membrane to be calculated by means of iterations. Once the solution has converged, the vapor flux through the membrane is calculated.

5.1. DCMD module

In software simulation of chemical processes, the first step is to define the feed streams in the system. In this case there are two, the seawater and permeate feed streams. Regarding the outputs there are also two streams, the one of the fed solution that does not pass through the membrane (rejected brine), and the output permeate stream. The resulting scheme is shown below.

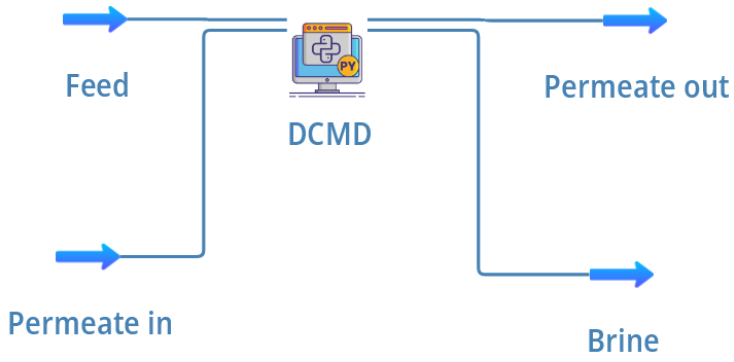

Figure 5.1. Schematic of a DCMD membrane module in DWSIM.

The permeate outflow corresponds to the sum of the fed permeate stream plus the flux through the membrane. Actually, for a first comparison of results, it is not necessary to calculate the permeate outflow. Therefore, for practical purposes, the flow across the membrane is set as an output stream, with the seawater feed stream being the sum of the two output streams.

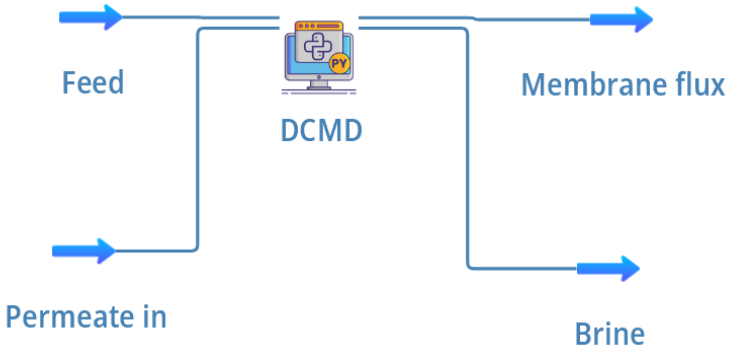

Figure 5.2. Simplified schematic of a DCMD membrane module in DWSIM for comparison purposes with the experimental fluxes.

It must be taken into consideration that in the simplified scheme above, the total mass flow fed is not equivalent to the total flow output. The objective in this first simulation is only to obtain the value of the flow through the membrane in order to compare it with the experimental values.

As previously done in the section on the validation of the mathematical model, the values of the different parameters and operating conditions are the same as those provided in the article followed [24]. In addition, the assumptions made previously are also taken into consideration. In this way, the conditions of the two feed streams in terms of temperature, pressure and volumetric flow rate are defined.

Regarding the salt composition in the seawater fed stream, the simulator works with mole and mass fractions, so the feed concentration of 38 g/L salt has been translated to a mass fraction of water of 0.9617. The calculation has been made from the correlation of the density calculation shown in Appendix A. The salt concentration of the fed permeate stream has been set initially as 0 g/L, so the mass fraction of water introduced is 1.

Subsequently, the mathematical model is introduced and the links between the code and the two fed and two output streams are created.

In solving the equations, the values of density, thermal conductivity, heat capacity and viscosity are required for the two feed streams. The DWSIM allows the values of these parameters to be obtained directly from the streams already defined, with the exception of viscosity. The viscosity values have been determined from the correlations used in the validation of the mathematical model. In addition, the values of this property at the temperatures of both membrane walls are also required. The correlation for the calculation of the conductivity of the vapor passing through the membrane is also introduced. Thus, a total of five correlations have been used in the code to estimate thermodynamic properties (four for viscosity and one for conductivity).

For the calculation of the mass balance of the flow stream passing through the membrane, the salt rejection offered by the membrane has to be defined within the code. Membranes used in desalination systems offer a high salt passage rejection close to 99%. Experimentally, the salt rejection value is determined from the concentration measurement in the feed and permeate streams.

$$R = \left(1 - \frac{c_p}{c_f}\right) \times 100 \tag{5.1}$$

In the article followed, the rejection of the membrane used has been experimentally determined, and the results obtained are shown below.

Table 5.1. Experimental salt rejection factors at different feed concentrations [24].

Feed concentration [g/L]	Salt rejection factor [%]
0.14	97.80
2	99.15
43	99.96
100	99.96

As can be seen, the salt rejection value does not vary significantly for the different feed concentrations studied. In order to perform the calculations, a constant value of salt rejection has to be assumed. In the present study it is intended to work at high salt concentrations of about 38 g/L, corresponding to the concentration in the Mediterranean Sea [8].

Of the concentrations studied experimentally in the table above, the one closest to 38 g/L is 43 g/L. As an approximation, the rejection obtained for the 43 g/L concentration is assumed, being the value of 99.96%.

Unlike the Excel model validation with correlations, the system is solved by iterating over only two variables (the temperatures on the two membrane walls), since the densities of the two feed streams are known. Once the simulation is running correctly, the results are compared with those obtained previously using only correlations as well as the experimental values.

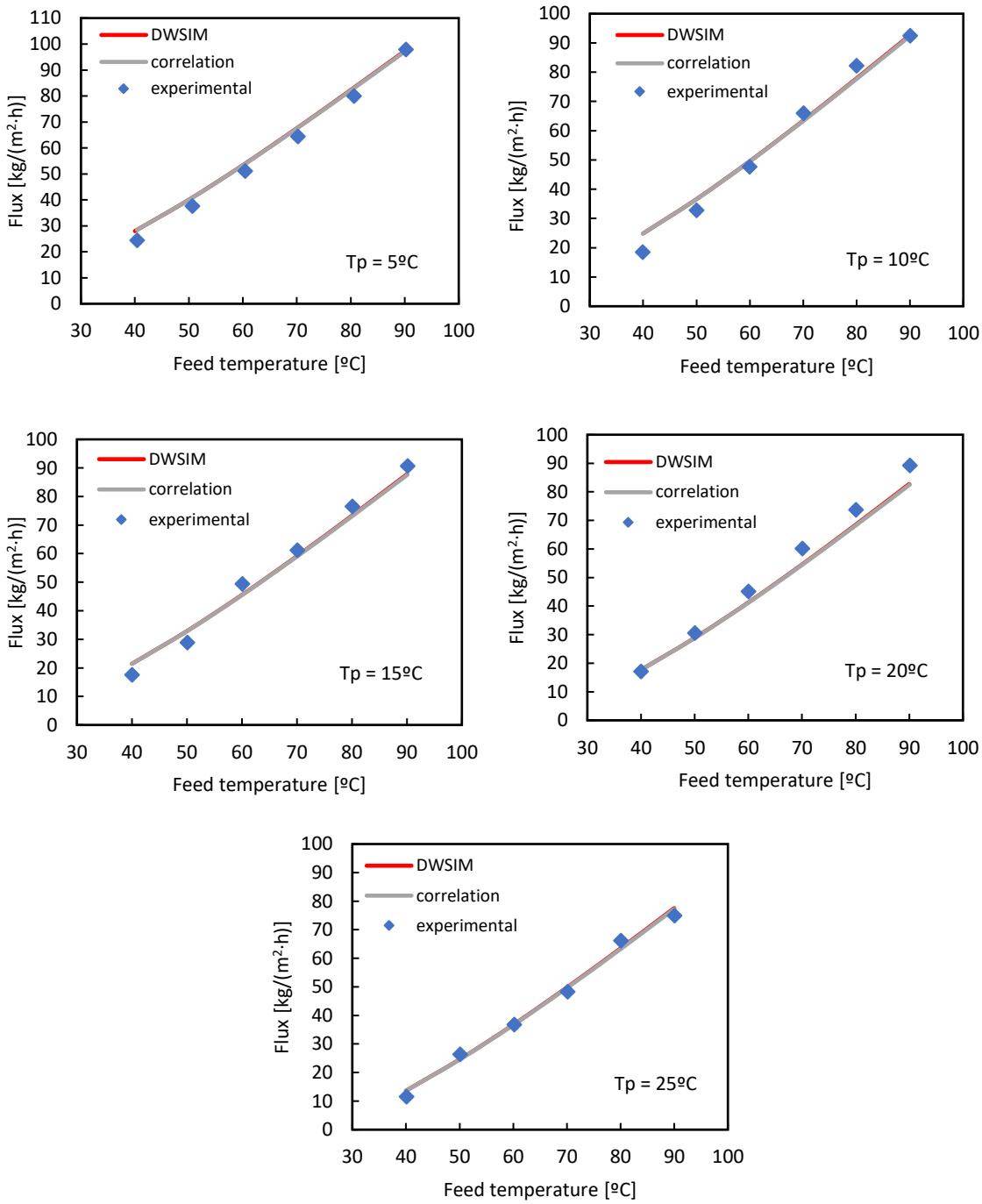

Figure 5.3. Fluxes through the membrane (experimental, by means of using correlations and by DWSIM) as a function of feed temperature for permeate temperatures of 5, 10, 15, 20 and 25ºC.

The results obtained with DWSIM clearly coincide with those determined with the validation of the mathematical model. However, with the current simulation it is not possible to determine the energy consumption of the DCMD process. For this, it is necessary to introduce other equipment such as the pumps, the heater and the cooler involved.

5.2. DCMD desalination system

In the following figure, the whole desalination process with DCMD technology is shown. The system consists of a feed stream which corresponds to the water to be desalinated or seawater (stream 1). And there are two outputs of the process, a stream of water with very low salt concentration (stream 8) and another with a higher concentration than the one provided (stream 10).

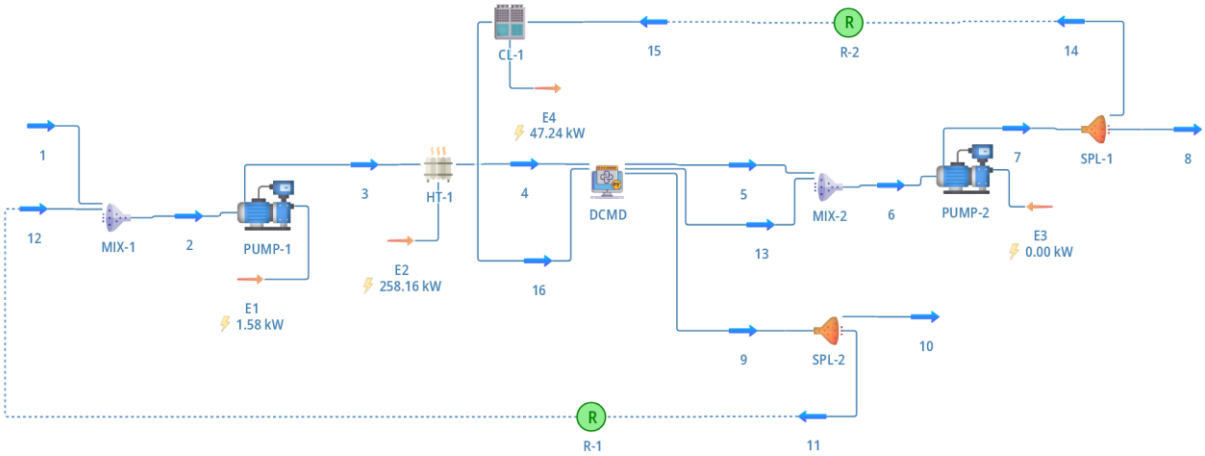

Figure 5.4. Schematic of a DCMD system of desalination in DWSIM.

Initially, there is a feed stream which corresponds to the seawater flow (stream 1). Subsequently, stream 1 is connected to stream 12 by means of a mixer to form stream 2, in which the pressure and temperature are increased. The resulting stream 4 is fed to the membrane module.

The stream 4 in the membrane module is divided into two streams, stream 5 which is the flow through the membrane, and stream 9 which is the rejected brine solution. Stream 9 is split in two, where a fraction leaves the system as an outflow (stream 10) and the other is fed back to the start of the process (stream 11 or 12).

In the membrane module three output streams can be observed, this is due to a simplification made. The permeate stream leaving the membrane module (stream 6) is the sum of the fed permeate stream (stream 13) plus the flux passing through the membrane (stream 5).

The calculation of this sum of streams could actually be performed within the Python code. However, for the sake of simplicity, this stream summation has been done "externally". Thus, within the code it was not necessary to implement the sum of the mass and energy balances of streams 5 and 13. So the permeate stream fed (stream 16) is exactly the same as stream 13.

On the other hand, stream 5 joins the fed permeate stream which is stream 13, giving rise to the output permeate stream which is stream 6. Stream 7 is divided into two streams, stream 8 which corresponds to the desalinated water output of the system, and stream 14 or 15 which is cooled to be fed back to the membrane module.

It is important to note that in this first scheme of the desalination process shown above, the pressure drop of the equipment and piping is not considered. Thus, as the permeate recirculation is a closed circuit, there is no pressure drop and therefore the pump on the permeate loop has no power consumption.

6. Optimization of working conditions from an energy point of view

In this section, an optimization study will be carried out for the different operating variables (temperature, pressure and split ratios) with respect to DCMD from an energy point of view. For this purpose, the configuration implemented in the DWSIM that include the different equipment present in the desalination system is used. In this way, the energy consumptions for the different cases can be determined.

In the simulation, the calculation basis is 1 kg/s, considering that the fed seawater stream has a concentration of 38 g/L, similar to that of the Mediterranean Sea [8].

One parameter of the mathematical model to be considered for the calculation basis used, is the membrane area. The area of the membrane depends on the flow rate of the feed flow. In the article followed [24], the membrane area is 0.06192 m^2 for a flow rate fed to the membrane module of 4.6 L/min. In this way, the flow rate fed to the membrane module divided by the unit of area can be calculated.

$$\frac{feed\ flowrate}{membrane\ area} = \frac{4.6\ L}{1\ \text{min} \times 0.06192\ m^2} \times \frac{1 min}{60\ s} = 1.238\ L/(s \times m^2) \tag{6.1}$$

Considering that one liter is approximately one kilogram, the value would be 1.238 kg/(s·m^2). If it is assumed that the flow rate fed to the membrane module is close to the flow rate fed to the process, the calculation of the equivalent area would be:

$$\frac{1\ kg}{1\ s \times [area] m^2} = \frac{1.238\ kg}{1\ s \times 1\ m^2} \tag{6.2}$$

By subtracting the area from the above equation, the value of 0.807 m^2 is obtained, which approximates an area of 0.8 m^2. Therefore, it is the value subsequently used in the simulation. Before conducting the sensitivity analysis, the following values of temperatures, pressures and ratios are assumed as a starting point and the range studied for the different variables.

Table 6.1. Initial values of the different variables to be studied.

Parameter	Initial value	Range studied
T_f	90ºC	40 to 90ºC
T_p	10ºC	10 to 30ºC
P_f	2.4 bar	1.5 to 5.0 bar
P_p	2.4 bar	1.5 to 5.0 bar
R_f	0.90	0.02 to 0.99
R_p	0.90	0.02 to 0.99

Due to the range of validity of the viscosity correlation implemented in the DCMD module code from 10 to 180°C, the minimum temperature defined for the permeate stream range is a value of 10°C.

The chosen temperature values as a starting point, produce the maximum flux through the membrane for the determined ranges, however, it is not known at this point whether the high energy consumption required for these conditions is optimal from an energy point of view.

6.1.1. Effect of temperature

The temperatures of the two streams fed into the membrane module are defined by the heater in the case of feed recirculation, and by the cooler in the case of permeate recirculation. According to the principle of operation of the DCMD technology, the greater the temperature difference, the higher the flux through the membrane, but on the other hand, the higher the energy consumption.

It is then determined whether it is really worth spending more energy to obtain a higher flow rate of desalinated water or not.

The following figure shows the steam flux through the membrane in [kg/(m²·h)] divided by the power consumed (kW) of the process equipment (heater, cooler and pump). All this, for a range of heater temperatures (from 40 to 90ºC) at different values of cooler temperatures.

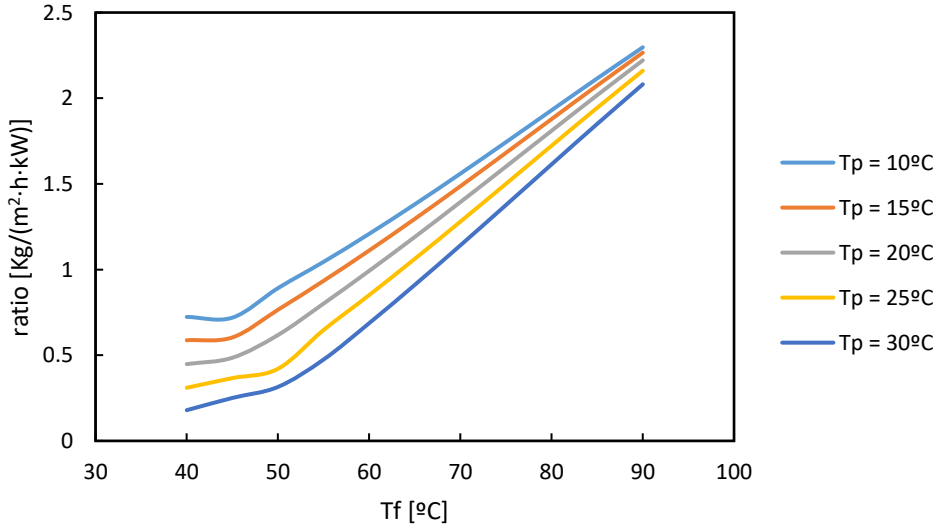

Figure 6.1. Fluxes divided by unit of power consumption as function of feed temperature for permeate temperatures of 10, 15, 20, 25 and 30ºC.

For the same power consumption, the flux through the membrane is higher for a high temperature in the feed stream and a low temperature in the permeate stream. For the values studied in this case, the optimum temperatures are 90ºC for the hot loop and 10ºC for the cold loop, where the ratio obtains a maximum value of 2.2972 kg/(m²·h·kW). Therefore, the initial temperature values chosen above have turned out to be optimal.

For low feed stream temperatures (approximately 40 to 50°C), the curves shown have a different trend. This is due to the fact that initially the permeate recirculation is in laminar regime. As the temperature of the feed stream increases, the flow through the membrane increases and so does the flow rate of the permeate recirculation. Thus, the flow velocity increases, increasing the Reynolds number value, giving rise to a turbulent regime.

The following figure shows how the mass flow rate of the permeate fed to the membrane module varies for the different temperatures studied.

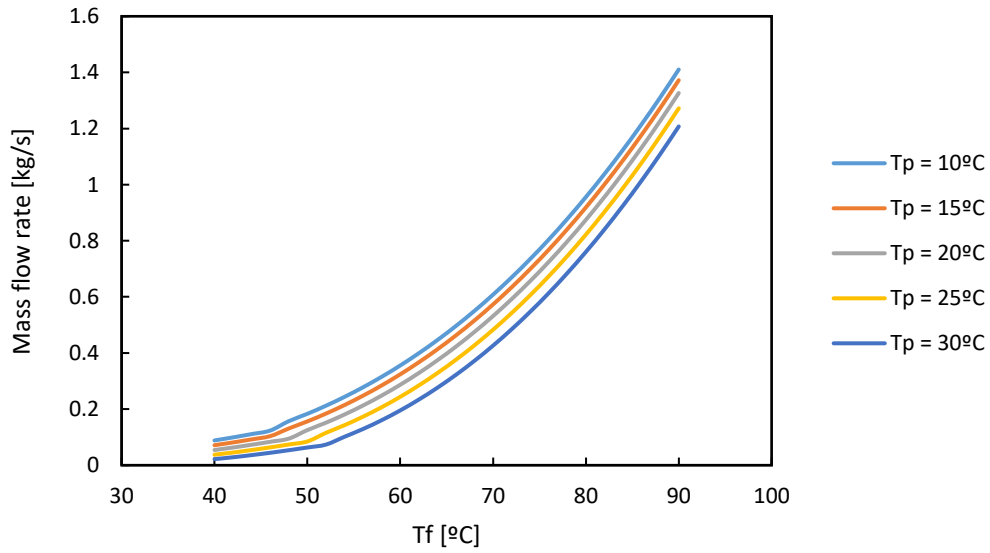

Figure 6.2. Mass flow rate of the permeate stream fed to the membrane module as function of feed temperature for permeate temperatures of 10, 15, 20, 25 and 30ºC.

The greater the temperature difference between the two inlet streams to the membrane module, the higher the permeate flow rate. Considering a constant ratio of 0.9 in the permeate recirculation, the flow rate increases rapidly at more favorable temperature conditions. This increases the convection coefficients and the energy transfer on both sides of the membrane.

The mathematical model has defined the change of regime from laminar to turbulent for a Reynolds value of 2300, so in the following figure, the change of behavior is clearly observed when reaching the mentioned value.

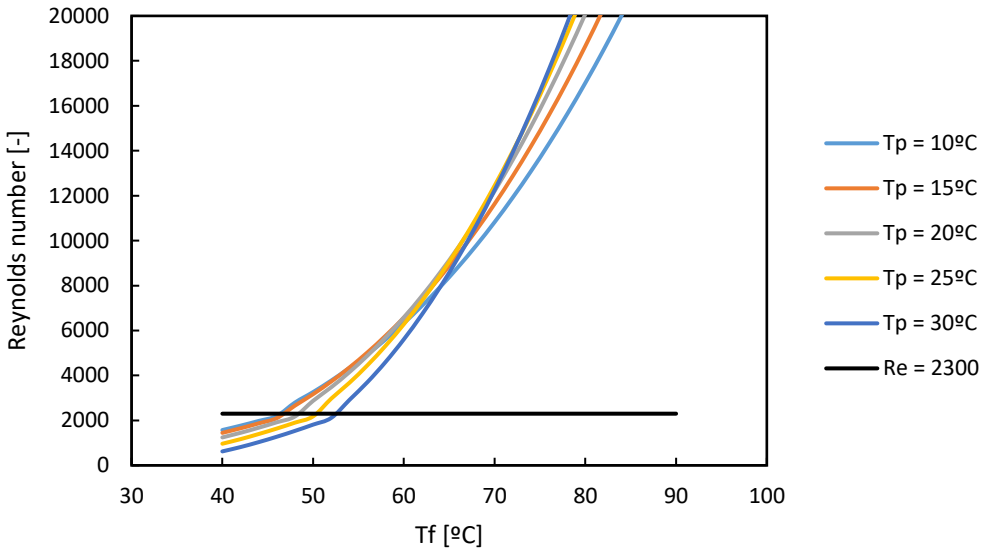

Figure 6.3. Reynolds number of the permeate stream fed to the membrane module as function of feed temperature for permeate temperatures of 10, 15, 20, 25 and 30ºC.

As expected, when the Reynolds number exceeds the value of 2300, a change of trend occurs, and the system behaves differently. The lines represented in the graph above change to a turbulent regime between the temperatures of approximately 40 and 50ºC of the feed recirculation temperature. These values are consistent with the temperature range in which the change in trend occurs, as seen in the Figure 6.1.

In this case, the results obtained are shown, but for the same amount of desalinated water instead for the same power consumption. The figure below shows the energy consumption of the process in kilowatt-hour for one kilogram of desalinated water produced.

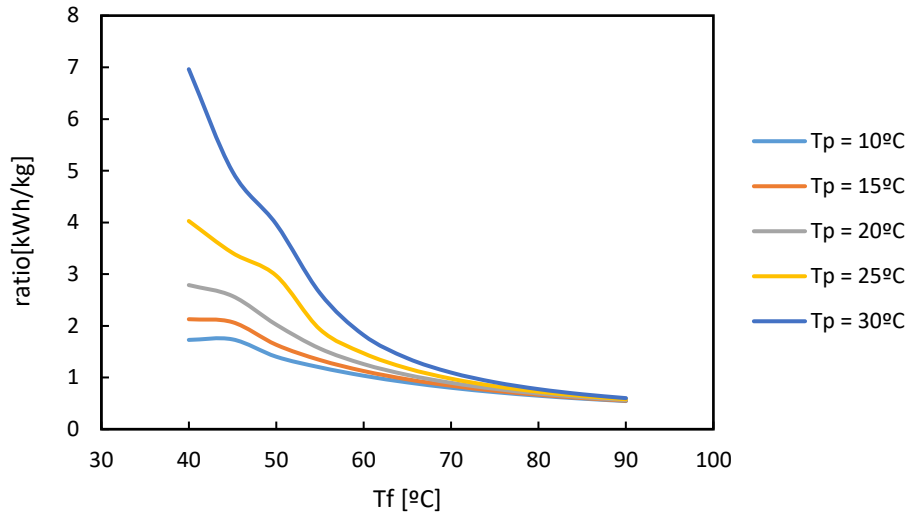

Figure 6.4. Energy consumption divided by kilogram of desalinated water produced as function of feed temperature for permeate temperatures of 10, 15, 20, 25 and 30ºC.

For high temperatures in the feed recirculation, it is observed that the temperature of the permeate recirculation is not very relevant. On the other hand, for low temperatures, the temperature of the permeate stream makes a big difference in the results obtained. As previously determined, the optimum conditions are at a feed recirculation temperature of 90ºC and a permeate recirculation temperature of 10ºC, giving optimum results of 0.54413 kWh/kg.

6.1.2. Effect of pressure

In the process, there are two pumps that regulate the pressures of the two inlet streams in the membrane module. However, in the simulation carried out, the pressure drop in the pipes is not considered. Therefore, the pump in the permeate recirculation has a consumption of 0 kW.

It is important to remember that, in solving the mathematical model of the membrane module unit, only the Knudsen diffusion coefficient is considered. This is due to a hypothesis carried out in the validation of the model, in which it has been determined that the contribution of molecular diffusion decreases the values of the fluxes through the membrane away from the experimental values. Knudsen diffusion is not influenced by the effect of pressure, but molecular diffusion is, because it depends on the partial pressure exerted by the air inside the membrane pores. Therefore, in this analysis of the effect of system pressure, it is to be expected that a higher pressure only contributes to a higher consumption by the pump, without providing any increase in the flux through the membrane. The results obtained are shown below.

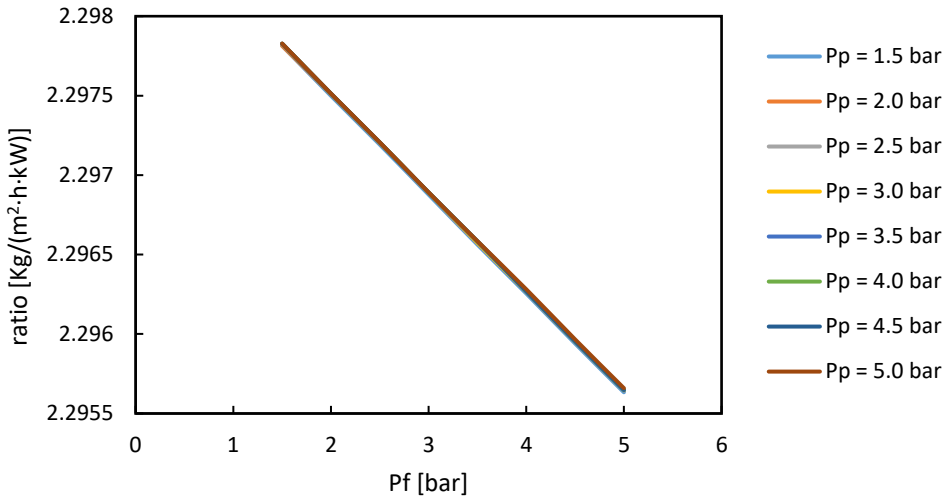

Figure 6.5. Fluxes divided by unit of power consumption as function of feed pressure for permeate pressures of 1.5, 2.0, 2.5, 3.0, 3.5, 4.0, 4.5 and 5.0 bar.

As pressure does not affect membrane performance, the ratio of flux divided by power unit decreases for higher pressures. In this case, the optimum pressure is the lowest studied (1.5 bar), where the ratio gets a value of 2.2978 kg/(m²·h·kW).

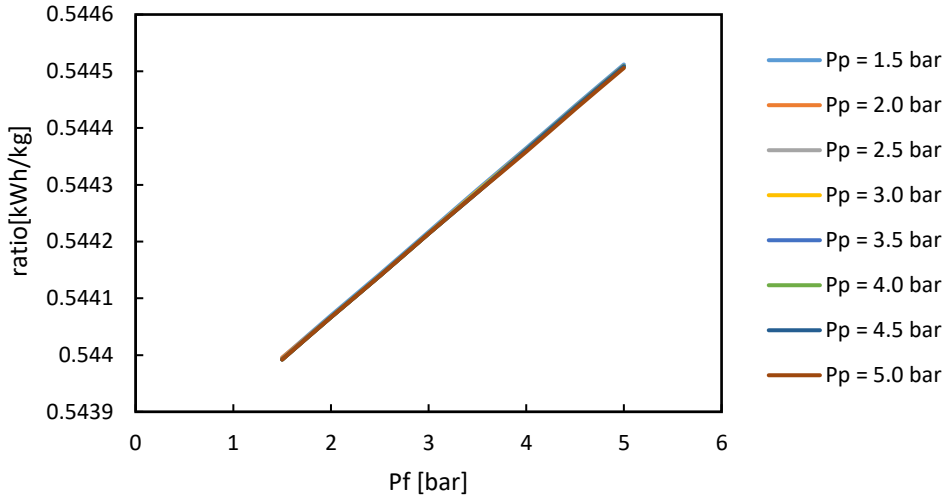

Figure 6.6. Energy consumption divided by kilogram of desalinated water produced as function of feed pressure for permeate pressures of 1.5, 2.0, 2.5, 3.0, 3.5, 4.0, 4.5 and 5.0 bar.

The energy consumption for one kilogram of desalinated water obtained is 0.54400 kWh/kg. The results obtained from the ratios are very similar to those obtained previously for the temperature study, being more favorable in the case of pressure optimization. Due to the reduction of the operating pressure of the two pumps from

2.4 to 1.5 bar. In the case of temperature, the optimum values have coincided with those established as initial values.

The pump consumption has been reduced from 1.58 kW (for the initial 2.4 bar case) to 0.55 kW (for the 1.5 bar case), but almost all of the energy consumption comes from the heater and the chiller. At optimum pressure, the combined consumption of both is 306.3 kW.

6.1.3. Effect of split ratios

The flow rates of the feed and permeate loops are affected by two stream separators or splitters. These significantly affect the performance of the system itself and the consumption of the different equipment involved.

A higher flow rate implies a higher consumption by the pump. But, on the other hand, it also implies a higher flow velocity, which results in a higher turbulence or Reynolds number. Thus, convection is favored on both sides of the membrane increasing the flux value. Also, the higher the flow rate, the smaller the temperature change in the recirculation stream, so the inlet temperature at the heater and cooler will be closer to the desired temperature.

By solving the simulation for different values of separation in the two splitters involved, the following results are obtained. Where R_f corresponds to the ratio of the feed recirculation and R_p to that of the permeate recirculation.

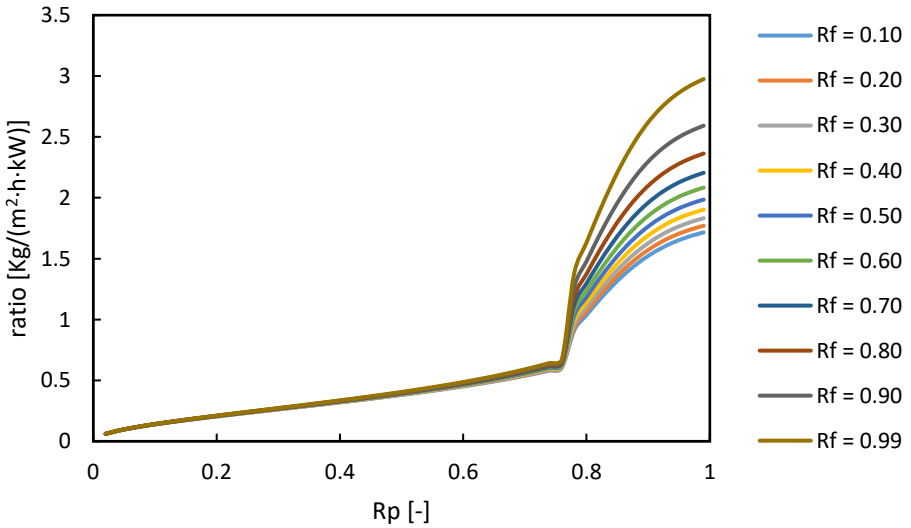

Figure 6.7. Fluxes divided by unit of power consumption as function of permeate split ratio for feed split ratios of 0.10, 0.20, 0.30, 0.40, 0.50, 0.60, 0.70, 0.80, 0.90 and 0.99.

When the value of the recirculation ratio of the permeate stream reaches 0.78, the Reynolds number exceeds the value of 2300, so it passes to the turbulent regime. At this point, the represented curves undergo a large change in their trend and the value of the feed recirculation significantly influences the membrane performance.

Representing the same ratio of flux through the membrane divided by unit power as a function of the feed loop ratio in this case, the following results are obtained.

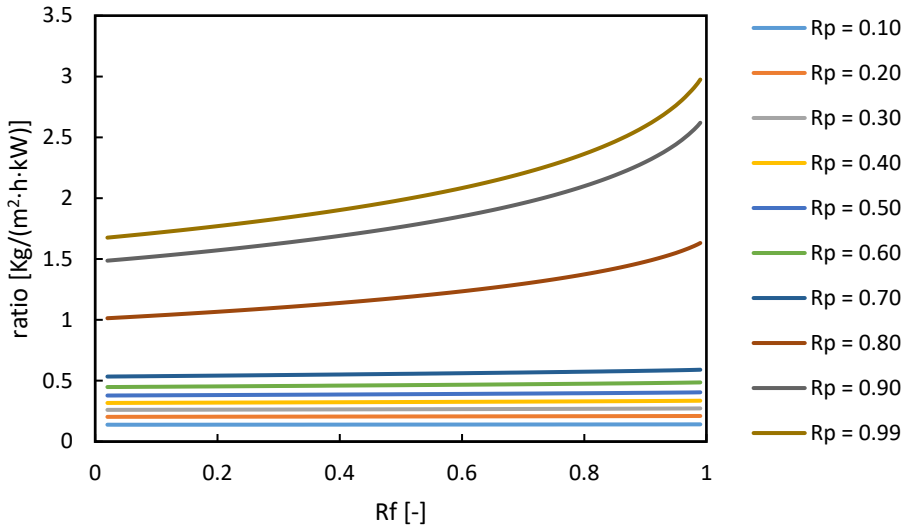

Figure 6.8. Fluxes divided by unit of power consumption as function of feed split ratio for permeate split ratios of 0.10, 0.20, 0.30, 0.40, 0.50, 0.60, 0.70, 0.80, 0.90 and 0.99.

The previous figure also shows the change from laminar to turbulent regime. For R_p values higher than 0.70, the curves represented modify their original trend favoring a higher flow for the same energy consumption. Therefore, it is convenient to operate at high recirculation flow rates for both feed and permeate, in order to optimize the energy consumption in the process.

From the values studied, the optimum point is when both R_f and R_p have the maximum value, which in this case is 0.99 ratios for both. This gives results of 2.9752 kg/(m²·h·kW). If the energy consumption divided by kilogram of desalinated water is plotted, the results obtained are as follows.

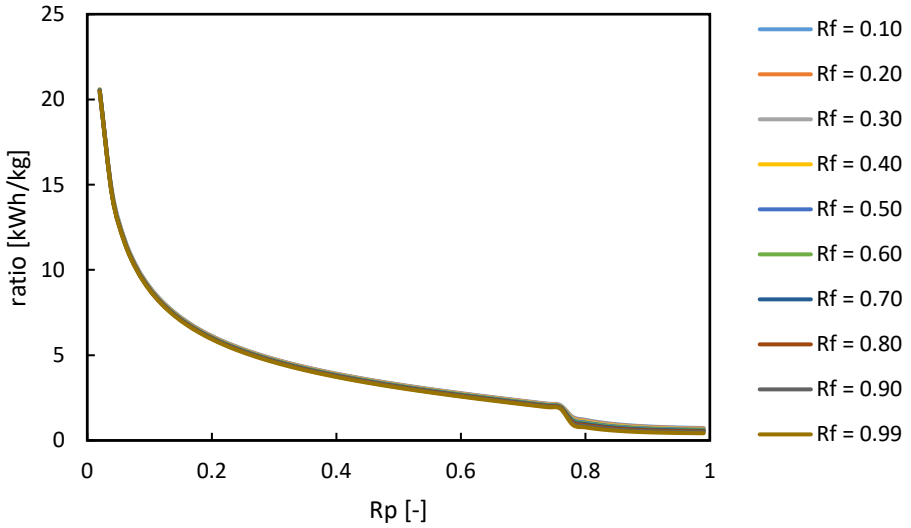

Figure 6.9. Energy consumption divided by kilogram of desalinated water produced as function of permeate split ratio for feed split ratios of 0.10, 0.20, 0.30, 0.40, 0.50, 0.60, 0.70, 0.80, 0.90 and 0.99.

The R_f value affects more the energy efficiency of the system for R_p values higher than 0.78, in other words, when the permeate recirculation is in turbulent regime. In contrast, the R_p ratio presents a large change in the results for values lower than 0.2. For the optimum conditions (when R_f and R_p have values of 0.99), the energy consumption is 0.42013 kWh/kg.

6.1.4. Best conditions

Once the different sensitivity analyses have been carried out to study the behavior of the DCMD system, the following optimum conditions have been determined for the studied ranges of the different variables.

Table 6.2. Optimal values of the different variables studied from an energy point of view.

Parameter	Optimal value	Range studied
T_f	90ºC	40 to 90ºC
T_p	10ºC	10 to 30ºC
P_f	1.5 bar	1.5 to 5.0 bar
P_p	1.5 bar	1.5 to 5.0 bar
R_f	0.99	0.02 to 0.99
R_p	0.99	0.02 to 0.99

For these conditions, the flux divided by power unit is 2.9759 kg/(m²·h·kW), and the energy required per kilogram of desalinated water is 0.42004 kWh/kg.

These results are similar as those previously obtained for the optimization of the R_f and R_p ratios. The difference is that for the optimum case, the pumps operating pressure is 1.5 bar instead of 2.4 bar. Numerically, the reduction of the pump consumption does not practically modify the results obtained previously, since its consumption is much lower than that of the heater and cooler.

Next, for the optimum conditions determined, the influence of the feed concentration will be observed, where in the previous analyses it has been considered to be 38 g/L. The range of feed concentrations for the following cases is 10 to 80 g/L.

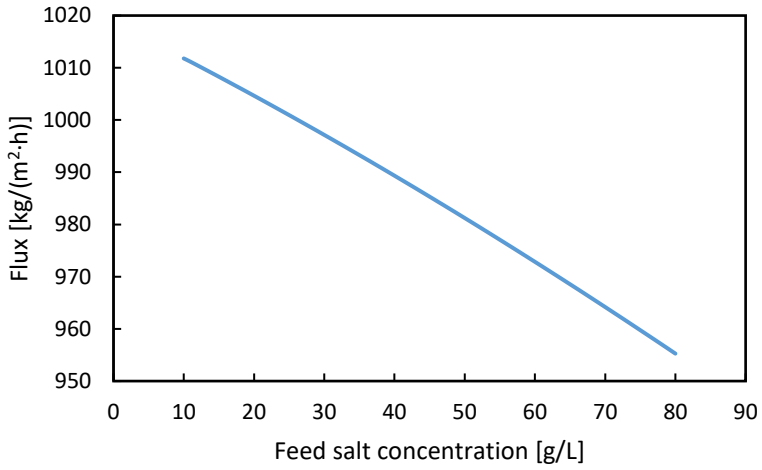

Figure 6.10. Flux through the membrane as function of feed salt concentration.

As shown in the figure above, as the salt concentration in the solution fed to the process increases, the vapor flux through the membrane is progressively reduced. This is due to the decrease in the water mole fraction, which results in a lower vapor pressure on the feed side. However, considering the energy consumption of the process itself, it is more favorable to operate at high salt concentrations as shown in the following two figures.

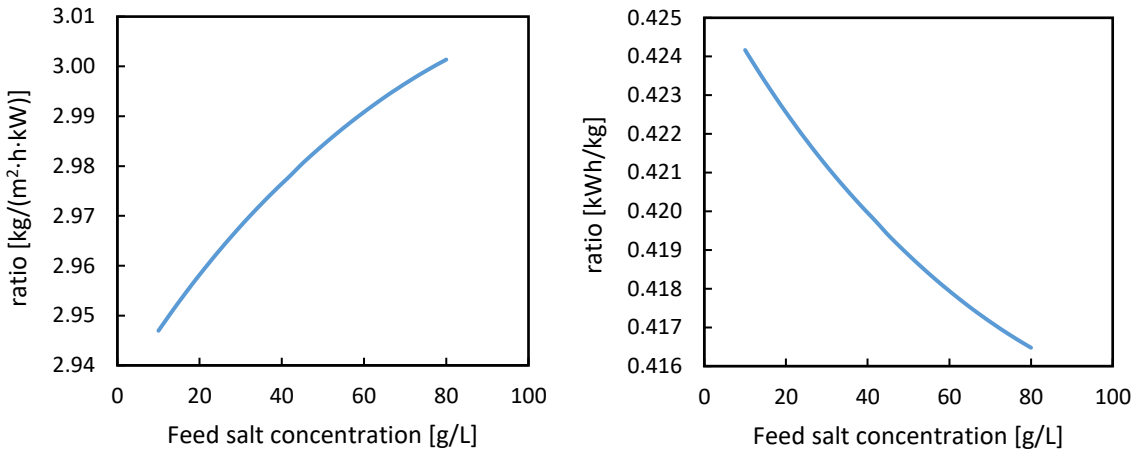

Figure 6.11. Fluxes divided by unit of power consumption and energy consumption divided by kilogram of desalinated water produced as function of feed salt concentration respectively.

For a salt concentration of 80 g/L, for each kilowatt of power consumed, a flux through the membrane of 3.00 kg/(m²·h) is obtained. Likewise, for each kilogram of desalinated water, about 0.416 kWh are consumed. The high salt concentration reduces the heat capacity value, so the heater and the cooler reduce their consumption significantly. Of the two equipment, the heater works at a higher flow rate, so that the decrease in heat capacity is more noticeable in the consumption of it.

The following figure shows how the increase in salt concentration in the feed affects both the power consumption of the heater and the heat capacity.

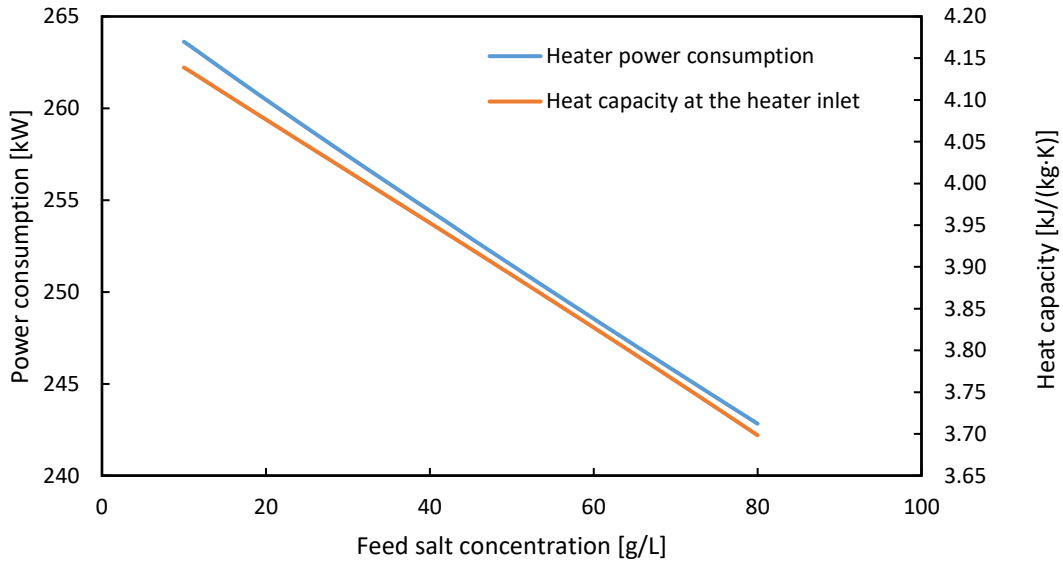

Figure 6.12. Power consumption by the heater, and heat capacity value at heater's feed stream, as function of the feed salt concentration.

Over the range of concentrations studied from 10 to 80 g/L, the heat capacity value has been reduced by 10.6% and the energy consumption in the heater by 7.89%. On the other hand, the increase in density due to the increase in salt concentration caused a 1.60% increase in the mass flow rate in the feed recirculation.

7. DCMD pilot plant study

In order to obtain results closer to reality, in this section the same simulation of the desalination process using DCMD technology will be carried out, but this time, considering the head loss present in pipes and elbows. For this purpose, the chemical process simulator DWSIM is used as before, which allows the calculations to be carried out automatically.

7.1. Pipe sizing and insulation

As a first step, it is necessary to establish the diameters of the pipes involved in the process. The diameters can be estimated from the volumetric flow rates obtained from the simulation studied previously, in which the head loss has not been considered. However, it is important to consider that not all streams in the process have to be taken into account. In each recirculation, the simulator creates a second stream to converge the solution of the recirculation itself, so the same current is duplicated (streams number 12 and 15). Moreover, in the process studied, in order to simplify the membrane module code, two streams have been defined that do not really exist (streams number 5 and 13).

The streams for which pipe sizing is not required are shown below. These are, as mentioned above, streams 5, 12, 13 and 15.

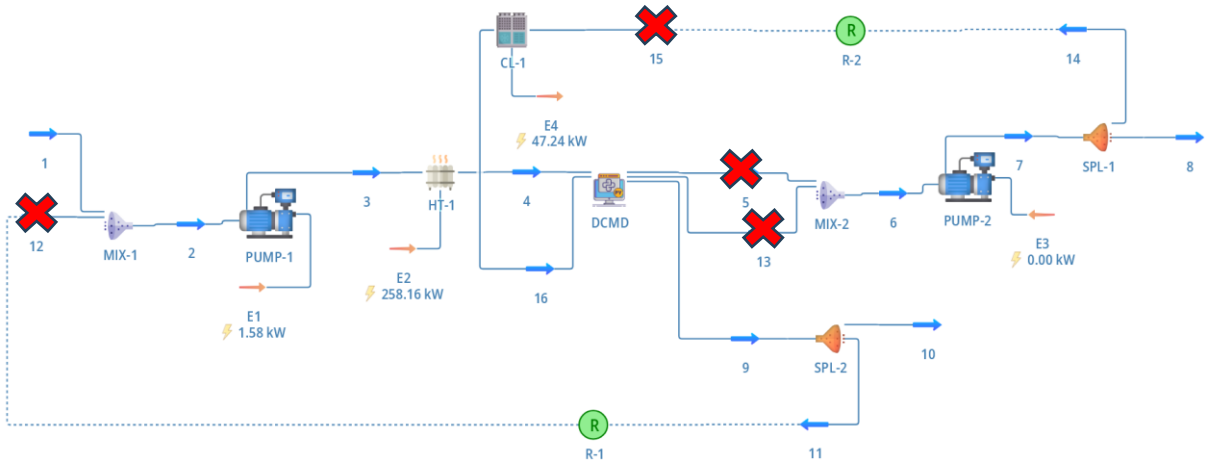

Figure 7.1. Schematic of a DCMD system of desalination in DWSIM with fictitious material streams marked.

Thus, the new distribution of the streams to be sized is as follows. In total, 12 pipes are required to be dimensioned to make up the desalination system.

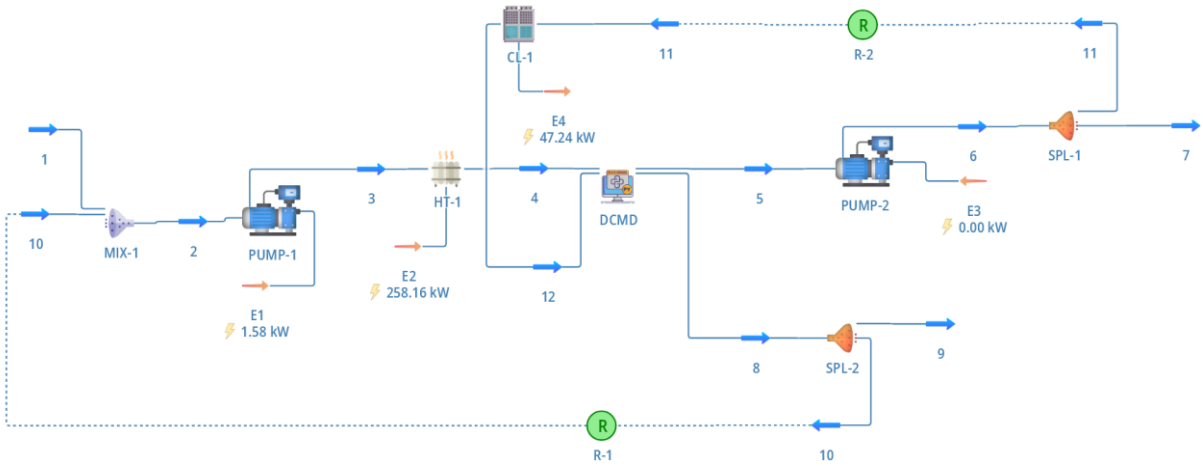

Figure 7.2. Schematic of a DCMD system of desalination in DWSIM with the material streams present in a possible pilot plant.

From the table of pipe profiles that follow the ASME B 36.10M standard [32], the pipe diameters are chosen so that the flow velocity is between 1 and 3 meters per second. This corresponds to the usual operating speed range for fluids in liquid phase in pipes.

In the process, there are pipes that operate at temperatures of around 90ºC and, on the other hand, there are pipes that work at temperatures of around 10ºC. In order to minimize the loss of energy from the fluid to the environment by radiation, an assessment is made of the pipes that require thermal insulation. To this end, it is established that flows with a temperature higher than 60ºC require heat insulation, and those with a temperature below 12ºC require cold insulation.

The table below shows the volumetric flow rates obtained by simulation for the 12 streams and the pipe diameters chosen for each case, as well as the resulting flow velocities. The operating temperatures and whether the pipes require insulation are also shown.

Table 7.1. Results obtained in the sizing of the DCMD desalination system piping and considering currents requiring thermal insulation.

Stream	Volumetric flow rate [L/s]	Nominal pipe size [inch]	Nominal diameter [mm]	Fluid velocity [m/s]	Temperature [ºC]	Insulation
1	0.974	1	25	1.75	25.0	No
2	78.0	10	250	1.53	89.2	Yes
3	78.0	10	250	1.53	89.2	Yes
4	78.0	10	250	1.53	90.0	Yes
5	22.0	6	150	1.18	10.8	Yes
6	22.0	6	150	1.18	10.8	Yes
7	0.220	1	25	0.39	10.8	Yes
8	77.8	10	250	1.53	90.0	Yes
9	0.778	1	25	1.40	90.0	Yes
10	77.0	10	250	1.51	90.0	Yes
11	21.8	6	150	1.17	10.8	Yes
12	21.8	6	150	1.17	10.0	Yes

It can be seen that for the chosen diameters, all the streams have a velocity between 1 and 2 meters per second, with the exception of stream 7. However, for practical purposes, in the industry it is not usual to work with diameters smaller than one inch. It has therefore been decided to follow this criterion and set the diameter at the above-mentioned size. Only from three different sizes of 1, 6 and 10 inch profiles, the entire pipe system can be dimensioned. More detailed information on the 1 to 10 inch pipe profiles can be found in Appendix D. Regarding pipe insulation, fiberglass is the material used for this case. Where the thickness of it is to be about one inch.

7.2. Pipe material

Once the diameters have been established, a suitable material has to be chosen. The DWSIM incorporates the characteristics of different materials for the calculation of the head loss in pipes. These include raw steel, carbon steel, cast iron, stainless steel, PVC, PVC + PFRV and commercial copper. In addition, it is also possible to define a material according to the user's needs by specifying the roughness and thermal conductivity values of the material. In this case, due to the strong corrosion caused by the presence of salt in the system, and the operating temperatures of up to 90ºC, it is established that the different pipe sections are made of stainless steel.

7.3. Results

Finally, it remains to define the length of the streams involved and to establish the required elbows. All this is established using AutoCAD® graphic design software. A design of the desalination process itself is made, in which the distances of the different pipe sections are measured. The diagram mentioned above can also be found in Appendix D.

For the current plant with a feed capacity of 1 kg/s or about 3600 kg/h, it is assumed that the unit of measurement dimensioned in the diagram is equivalent to its value multiplied by two in centimeters. Thus, a dimensioned distance of 30 units would be equivalent to a length of 60 centimeters. Following this relationship, all the lengths of the different pipes together with the elbows involved in the process are entered into the software. As a hypothesis, it is assumed that all pipes are at the same height with respect to the ground.

Once all parameters have been set, the simulation is performed for the optimum conditions defined in the previous section in order to compare the results obtained. Appendix D shows the resulting scheme of the process in the simulation environment. The most relevant results obtained for the different pipe sections are shown below.

Table 7.2. Results obtained in the sizing of the DCMD desalination system piping.

Stream	Distance [m]	Number of elbows 90º	Heat loss [W]	Pressure drop [Pa]	Head loss [Pa/m]
1	0.700	-	~ 0	1067	1520
2	0.600	-	14.5	52.43	87.4
3	0.600	-	14.4	52.43	87.4
4	0.600	-	20.2	49.95	83.3
5	0.600	-	1.59	50.33	83.9
6	0.600	-	1.59	50.33	83.9
7	0.700	-	~ 0	71.71	102
8	0.600	-	20.7	49.68	82.8
9	5.045	2	0.706	8629	1710
10	3.394	2	69.8	1591	469
11	1.912	2	5.35	918.9	481
12	0.600	-	1.70	49.56	82.6

For each pipe section, regarding the calculation of heat loss, the transfer of energy from the fluid to the pipe by means of convection, conduction through the stainless steel and the thermal insulator, and finally, convection and radiation from the insulator to the ambient air at a temperature of 25ºC has been considered.

In total, an estimated energy loss of the system is about 150.5 Watts. Regarding the pressure drop, this value is about 12632 Pa or about 0.13 bar. These results have minimally affected the consumption of the different equipment as can be seen in the following table.

Table 7.3. Comparative results of the DCMD desalination process at the energetically optimal conditions, considering or not the head and heat loss in the pipe sections.

	Without head and heat loss	With head and heat loss
Flux [kg/(m²·h)]	989.88	989.88
Heater power consumption [kW]	254.63	254.66
Cooler power consumption [kW]	72.941	72.982
Feed loop pump power consumption [kW]	5.0625	5.1799
Permeate loop pump power consumption [kW]	0	0.03137
Ratio [kg/(m²·h·kW)]	2.9759	2.9740
Ratio [kWh/kg]	0.42004	0.42031

As expected, the flux through the membrane is not affected by the pressure drop of the system, as the flux does not depend on the pressure when considering only Knudsen diffusion. With regard to the energy consumption of the different equipment, the values are actually very similar. For all of them, the energy consumption has slightly increased for the case in which the pressure drop in the pipes is considered. The pump located in the feed recirculation suffers an increase in power consumption of 117.3 W, the highest recorded. This change is due to the fact that the pressure at which the pump is fed is reduced from 101325 to 100206 Pa. In the case of the other pump, the pressure loss in the permeate recirculation due to friction is only 1069 Pa, so its power consumption is remarkably low. Moreover, the efficiency ratios obtained are very similar, being slightly more unfavorable for the case where the head and heat loss is taken into account.

These results show the low relevance of the consideration of head and heat loss in the system. Therefore, the sensitivity analyses carried out in the energy optimization section could neglect the presence of these phenomena.

Appendix D shows a Process Flow Diagram (PFD) with the operating conditions of the different streams as well as the temperature, pressure, mass flow rate and mass fraction of the simulation carried out.

8. Conclusions

In this project, a successful study of one of the desalination technologies increasingly present and used in industry has been carried out. A mathematical model has been developed, implemented and validated with experimental results. The energy optimization of the operating conditions by means of the DWSIM software has made it possible to reduce its consumption from 0.54413 to 0.42004 kWh for each kilogram of desalinated water. This reduction represents a decrease of 22.8%. Furthermore, considering the system head loss and the loss of energy to the environment, the results obtained are 0.42031 kWh/kg for the assumptions made. All this for a concentration of water to be desalinated of 38 g/L considering a calculation basis of 1 kg/s.

However, the energy consumption results obtained are significantly higher than the energy consumption required in other desalination processes, such as reverse osmosis. With reverse osmosis, the energy cost ranges between 2 and 3 kWh per cubic meter of water produced. Nevertheless, the advantage of DCMD is that it allows residual heat from other processes to be used. Therefore, the heater used in the DCMD process can be replaced using any equivalent waste energy source. Moreover, as it has been seen in the study of the temperature effect, for heater operating temperatures close to 90ºC, very similar results can be obtained without even the cooler also involved in the process. Therefore, water could only be desalinated by supplying energy to the pumps. The key is to make good use of a source of waste energy.

Under these conditions, DCMD technology offers great desalination possibilities at minimal energy costs and can even compete with current commonly used technologies such as reverse osmosis.

9. References

[1] Fundación AQUAE, ¿Qué industrias consumen más agua?, last update: 23/08/2021 https://www.fundacionaquae.org/que-industrias-consumen-mas-agua/ [consulted: 14/03/2024]

[2] Naciones Unidas, El número y la duración de las sequías han aumentado un 29% desde el año 2000, last update: 12/05/2022 https://news.un.org/es/story/2022/05/1508622 [consulted: 14/03/2024]

[3] Wikipedia, Water scarcity, Map of global water stress, 2019 https://en.wikipedia.org/wiki/Water_scarcity#/media/File:Water_stress_2019_WRI.png [consulted: 14/03/2024]

[4] United States Environmental Protection Agency, Drinking water requirements for States and public water systems, Drinking water regulations, last update: 30/11/2023. https://www.epa.gov/dwreginfo/drinking-water-regulations [consulted: 15/04/2024]

[5] United States Environmental Protection Agency, Ground water and drinking water, National primary drinking water regulation table, May 2009 https://www.epa.gov/sites/default/files/2016-06/documents/npwdr_complete_table.pdf [consulted: 15/04/2024]

[6] United Nations, Sustainable development goals, Goal 6: Ensure access to water and sanitation for all, 2023. https://www.un.org/sustainabledevelopment/water-and-sanitation/ [consulted: 14/03/2024]

[7] Statista, Economics & Politics, World: Total population from 2012 to 2022, last update: 2022. https://www.statista.com/statistics/805044/total-population-worldwide/ [consulted: 14/03/2024]

[8] Li NN. Advanced membrane technology and applications. Hoboken, N.J: Wiley; 2008.

[9] El-Dessouky HT, Ettouney HM. Fundamentals of salt water desalination. Amsterdam [etc: Elsevier; 2002.

[10] Curto D, Franzitta V, Guercio A. A Review of the Water Desalination Technologies. Applied sciences. 2021;11(2):670-. DOI: 10.3390/app11020670

[11] Baker RW (Richard W. Membrane technology and applications. 3rd ed. Chichester, West Sussex: John Wiley; 2012.

[12] Kucera J. Reverse osmosis : design, processes, and applications for engineers. Salem, MA: Scrivener Pub.; 2010.

[13] Iagua, ¿Qué es una IDAM?
https://www.iagua.es/respuestas/que-es-planta-desaladora-agua-mar
[consulted: 09/04/2024]

[14] International Desalination and Reuse Association, Impact in numbers created through Desalination and Water Reuse, 2024
https://idadesal.org/ [consulted: 27/05/2024]

[15] Iagua, El know-how español en desalinización, un referente a nivel mundial, last update: 25/02/2022
https://www.iagua.es/noticias/redaccion-iagua/know-how-espanol-desalinizacion-referente-nivel-mundial [consulted: 09/04/2024]

[16] Fundación AQUAE, Cifras sobre la desalinización, last update: 25/08/2021
https://www.fundacionaquae.org/wiki/cifras-sobre-la-desalinizacion/
[consulted: 09/04/2024]

[17] Fundación AQUAE, Plantas desaladoras en España, last update: 26/02/2024
https://www.fundacionaquae.org/wiki/plantas-desaladoras-en-espana/
[consulted: 09/04/2024]

[18] Wikipedia, Brackish water, last update: 16/03/2024
https://en.wikipedia.org/wiki/Brackish_water [consulted: 09/04/2024]

[19] AEDYR, Asociación Española de desalación y reutilización, last uptade: 11/02/2019
https://aedyr.com/cifras-desalacion-espana/ [consulted: 09/04/2024]

[20] Agencia Balear del Agua y la Calidad Ambiental, Red de infraestructuras de abastecimiento y desalación
https://abaqua.cat/es/seccio/xarxa-dinfraestructures-dabastament-i-dessalacio/
[consulted: 09/04/2024]

[21] Mustakeem, M., Soukane, S., Saqib Nawaz, M., & Ghaffour, N. (2022). Desalination by Membrane Distillation. IntechOpen. DOI: 10.5772/intechopen.101457

[22] Khayet Mohamed, Matsuura T. Membrane distillation : principles and applications. Amsterdam: Elsevier; 2011.

[23] Ameen NAM, Ibrahim SS, Alsalhy QF, Figoli A. Highly Saline Water Desalination Using Direct Contact Membrane Distillation (DCMD): Experimental and Simulation Study. Water (Basel). 2020;12(6):1575-. DOI: 10.3390/w12061575

[24] Khalifa A, Ahmad H, Antar M, Laoui T, Khayet M. Experimental and theoretical investigations on water desalination using direct contact membrane distillation. Desalination. 2017;404:22–34. DOI: 10.1016/j.desal.2016.10.009

[25] Phattaranawik J, Jiraratananon R, Fane AG. Heat transport and membrane distillation coefficients in direct contact membrane distillation. Journal of membrane science. 2003;212(1):177–93. DOI: 10.1016/S0376-7388(02)00498-2

[26] Qtaishat M, Matsuura T, Kruczek B, Khayet M. Heat and mass transfer analysis in direct contact membrane distillation. Desalination. 2008;219(1):272–92.
DOI: 10.1016/j.desal.2007.05.019

[27] Essalhi M, Khayet M. Self-sustained webs of polyvinylidene fluoride electrospun nanofibers at different electrospinning times: 2. Theoretical analysis, polarization effects and thermal efficiency. Journal of membrane science. 2013;433:180–91.
DOI: 10.1016/j.memsci.2013.01.024

[28] Iversen SB, Bhatia VK, Dam-Johansen K, Jonsson G. Characterization of microporous membranes for use in membrane contactors. Journal of membrane science. 1997;130(1):205–17. DOI: 10.1016/S0376-7388(97)00026-4

[29] Çengel, Yunus A., and Afshin J. Ghajar. Heat and Mass Transfer: Fundamentals and Applications. 5th ed., McGraw-Hill Professional, 2014.

[30] Winter, D. Membrane Distillation, A Thermodynamic, Technological and Economic Analysis. Ph.D. Thesis, University of Kaiserlautern, Kaiserlautern, Germany, 2014.

[31] Professional Plastics, Typical properties of PTFE.
https://www.professionalplastics.com/professionalplastics/content/Teflon_PTFE.pdf

[32] Tubing China, B36.10M, Dimensions and Weights of Welded and Seamless Wrought Steel Pipe, 2015.
https://tubingchina.com/ASME-B36.10M.pdf [consulted: 13/04/2024]

Appendix A – Estimation of thermodynamic properties

A.1. Properties of saturated water

Table A.1A. Properties of saturated water used in the DCMD model validation [29].

T [ºC]	ρ $[kg/m^3]$	C_p $[J/(kg \cdot K)]$	k_{liq} $[W/(m \cdot K)]$	k_{gas} $[W/(m \cdot K)]$	μ $[Pa \cdot s]$	Pr [-]
5	999.9	4205	0.571	0.0173	0.001519	11.2
10	999.7	4194	0.58	0.0176	0.001307	9.45
15	999.1	4185	0.589	0.0179	0.001138	8.09
20	998.0	4182	0.598	0.0182	0.001002	7.01
25	997.0	4180	0.607	0.0186	0.000891	6.14
30	996.0	4178	0.615	0.0189	0.000798	5.42
35	994.0	4178	0.623	0.0192	0.000720	4.83
40	992.1	4179	0.631	0.0196	0.000653	4.32
45	990.1	4180	0.637	0.0200	0.000596	3.91
50	988.1	4181	0.644	0.0204	0.000547	3.55
55	985.2	4183	0.649	0.0208	0.000504	3.25
60	983.3	4185	0.654	0.0212	0.000467	2.99
65	980.4	4187	0.659	0.0216	0.000433	2.75
70	977.5	4190	0.663	0.0221	0.000404	2.55
75	974.7	4193	0.667	0.0225	0.000378	2.38
80	971.8	4197	0.67	0.0230	0.000355	2.22
85	968.1	4201	0.673	0.0235	0.000333	2.08
90	965.3	4206	0.675	0.0240	0.000315	1.96
95	961.5	4212	0.677	0.0246	0.000297	1.85
100	957.9	4217	0.679	0.0251	0.000282	1.75

A.2. Thermodynamic properties estimated by correlations

Correlations used for the estimation of the thermodynamic properties in the validation of the mathematical model of the DCMD unit. The correlations of the dynamic viscosity, and thermal conductivity in the gas phase are also used in the resolution of the model by means of the DWSIM software.

Density [$\boldsymbol{\rho}$ *in* $\boldsymbol{kg/m^3}$]

Valid for salinity values (S) from 0 to 160 g/kg and temperatures from 10 to 180ºC (T) [30].

$$\rho = [0.5 \times a_0 + a_1 \times Y + a_2 \times (2 \times Y^2 - 1) + a_3 \times (4 \times Y^3 - 3 \times Y)] \times 1000 \quad \text{(A.1)}$$

$$a_0 = 2.01611 + 0.115313 \times \sigma + 0.000326 \times (2 \times \sigma^2 - 1) \quad \text{(A.2)}$$

$$a_1 = -0.0541 + 0.001571 \times \sigma - 0.000423 \times (2 \times \sigma^2 - 1) \quad \text{(A.3)}$$

$$a_2 = -0.006124 + 0.00174 \times \sigma - 0.000009 \times (2 \times \sigma^2 - 1) \quad \text{(A.4)}$$

$$a_3 = 0.000346 + 0.000087 \times \sigma - 0.000053 \times (2 \times \sigma^2 - 1) \quad \text{(A.5)}$$

$$Y = \frac{2 \times T - 200}{160} \quad \text{(A.6)}$$

$$\sigma = \frac{2 \times S - 150}{150} \quad \text{(A.7)}$$

Dynamic viscosity [$\boldsymbol{\mu}$ *in* $\boldsymbol{Pa \cdot s}$]

Valid for salinity values (S) from 0 to 130 g/kg and temperatures from 10 to 180ºC (T) [9] [30].

$$\mu = \mu_W \times \mu_R \times 10^{-3} \quad \text{(A.8)}$$

$$ln(\mu_W) = -3.79418 + \frac{604.129}{139.18 + T} \quad \text{(A.9)}$$

$$\mu_R = 1 + a_1 \times S + a_2 \times S^2 \quad \text{(A.10)}$$

$$a_1 = 1.474 \times 10^{-3} + 1.5 \times 10^{-5} \times T - 3.927 \times 10^{-8} \times T^2 \quad \text{(A.11)}$$

$$a_2 = 1.0734 \times 10^{-5} + 8.5 \times 10^{-8} \times T - 2.23 \times 10^{-10} \times T^2 \quad \text{(A.12)}$$

Heat capacity [C_p *in* $J/(kg \cdot K)$]

Valid for salinity values (S) from 0 to 160 g/kg and temperatures from 10 to 180ºC (T) [9] [30].

$$C_p = A + B \times T + C \times T^2 + D \times T^3 \quad \text{(A.13)}$$

$$A = 4206.8 - 6.6197 \times S + 1.2288 \times 10^{-2} \times S^2 \quad \text{(A.14)}$$

$$B = -1.1262 + 5.4178 \times 10^{-2} \times S - 2.2719 \times 10^{-4} \times S^2 \quad \text{(A.15)}$$

$$C = 1.2026 \times 10^{-2} - 5.3566 \times 10^{-4} \times S + 1.8906 \times 10^{-6} \times S^2 \quad \text{(A.16)}$$

$$D = 6.8777 \times 10^{-7} + 1.5170 \times 10^{-6} \times S - 4.4268 \times 10^{-9} \times S^2 \quad \text{(A.17)}$$

Thermal conductivity, liquid phase [k *in* $W/(m \cdot K)$]

Valid for salinity values (S) from 0 to 100 g/kg and temperatures from 10 to 150ºC (T) [30].

$$k = (A + B \times T + C \times T^2) \times 10^{-3} \quad \text{(A.18)}$$

$$A = 576.6 - 34.64 \times X + 7.286 \times X^2 \quad \text{(A.19)}$$

$$B = (1526 + 466.2 \times X - 226.8 \times X^2 + 28.67 \times X^3) \times 10^{-3} \quad \text{(A.20)}$$

$$C = -(581 + 2055 \times X - 991.6 \times X^2 + 146.4 \times X^3) \times 10^{-5} \quad \text{(A.21)}$$

$$X = \frac{28.17 \times S}{1000 - S} \quad \text{(A.22)}$$

Thermal conductivity, vapor phase [k *in* $W/(m \cdot K)$]

The vapor flux passing through the membrane has a significantly low salt concentration, as the membrane itself offers a high salt rejection. Therefore, as an approximation, the conductivity is considered equivalent to that of pure water.

The expression used for this case has been obtained by performing a regression from the values of the table of pure water properties. Where T_m corresponds to the average membrane temperature expressed in Kelvin.

$$\begin{aligned} k_{gas} = & -2.466012 \times 10^{-14} \times {T_m}^6 + 4.816868 \times 10^{-11} \times {T_m}^5 \\ & - 3.910949 \times 10^{-8} \times {T_m}^4 + 1.689556 \times 10^{-5} \times {T_m}^3 \\ & - 0.004095894 \times {T_m}^2 + 0.5283401 \times T_m - 28.31889 \end{aligned} \quad \text{(A.23)}$$

Appendix B – DCMD model validation results

A.3. Adjustment of the alpha parameter

Table A.1B. Fluxes through the membrane at different Knudsen and molecular diffusion contributions for a permeate temperature of 10ºC.

T_f [ºC]	Flux (experimental) [kg/(m²·h)]	Flux interp. α = 0.7 [kg/(m²·h)]	Flux interp. α = 0.8 [kg/(m²·h)]	Flux interp. α = 0.9 [kg/(m²·h)]	Flux interp. α = 1.0 [kg/(m²·h)]
39.94	18.56	11.60	14.11	17.99	24.74
50.02	32.82	19.33	22.97	28.27	36.57
59.96	47.73	29.20	33.89	40.30	49.43
70.04	65.97	41.48	47.01	54.10	63.35
79.98	82.21	55.57	61.56	68.82	77.59
90.06	92.49	71.46	77.51	84.44	92.31

A.4. Comparison with the experimental values

Table A.2B. Comparison of the estimated flux values (using pure saturated water properties and correlations) with the experimental fluxes, for T_p temperatures of 5, 10, 15, 20 and 25ºC.

T_p = 5ºC				
T_f [ºC]	Flux (experimental) [kg/(m²·h)]	Flux (interpolated) [kg/(m²·h)]	Flux (correlations) [kg/(m²·h)]	Error (flux with correlations) [%]
40.40	24.41	28.37	28.43	16.50
50.63	37.63	40.78	40.82	8.479
60.41	51.19	53.83	53.87	5.239
70.19	64.41	67.67	67.73	5.167
80.57	80.00	82.87	82.99	3.734
90.21	97.97	97.22	97.39	0.588

Table A.2B. Comparison of the estimated flux values (using pure saturated water properties and correlations) with the experimental fluxes, for T_p temperatures of 5, 10, 15, 20 and 25ºC. (cont.)

T_p = 10ºC				
T_f [ºC]	Flux (experimental) [kg/(m²·h)]	Flux (interpolated) [kg/(m²·h)]	Flux (correlations) [kg/(m²·h)]	Error (flux with correlations) [%]
39.94	18.56	24.74	24.80	33.58
50.02	32.82	36.58	36.60	11.54
59.96	47.73	49.43	49.46	3.606
70.04	65.97	63.36	63.39	3.912
79.98	82.21	77.59	77.66	5.539
90.06	92.49	92.36	92.44	0.049
T_p = 15ºC				
T_f [ºC]	Flux (experimental) [kg/(m²·h)]	Flux (interpolated) [kg/(m²·h)]	Flux (correlations) [kg/(m²·h)]	Error (flux with correlations) [%]
40.02	17.63	21.41	21.44	21.62
50.04	28.90	32.88	32.88	13.78
60.06	49.42	45.55	45.53	7.87
70.08	61.27	59.08	59.07	3.59
80.10	76.59	73.19	73.18	4.46
90.11	90.75	87.65	87.64	3.43
T_p = 20ºC				
T_f [ºC]	Flux (experimental) [kg/(m²·h)]	Flux (interpolated) [kg/(m²·h)]	Flux (correlations) [kg/(m²·h)]	Error (flux with correlations) [%]
40.02	17.09	17.67	17.68	3.47
50.04	30.61	28.89	28.87	5.70
60.06	45.15	41.30	41.24	8.67
70.08	60.20	54.58	54.49	9.48
80.10	73.72	68.46	68.34	7.30
90.11	89.29	82.69	82.56	7.53

Table A.2B. Comparison of the estimated flux values (using pure saturated water properties and correlations) with the experimental fluxes, for T_p temperatures of 5, 10, 15, 20 and 25ºC. (cont.)

T_p = 25ºC				
T_f [ºC]	Flux (experimental) [kg/(m²·h)]	Flux (interpolated) [kg/(m²·h)]	Flux (correlations) [kg/(m²·h)]	Error (flux with correlations) [%]
40.09	11.54	13.72	13.72	18.88
50.05	26.37	24.66	24.61	6.68
60.15	36.81	36.92	36.82	0.029
70.11	48.35	49.91	49.76	2.92
80.07	66.21	63.49	63.33	4.35
90.04	75.00	77.57	77.29	3.06

Table A.3B. Comparison of the estimated flux values (using pure saturated water properties and correlations) with the experimental fluxes, for T_f temperatures of 50, 70 and 90ºC.

T_f = 50ºC				
T_p [ºC]	Flux (experimental) [kg/(m²·h)]	Flux (interpolated) [kg/(m²·h)]	Flux (correlations) [kg/(m²·h)]	Error (flux with correlations) [%]
5.010	37.56	39.98	40.01	6.53
10.02	33.10	36.54	36.57	10.46
15.02	30.88	32.82	32.82	6.30
20.03	30.56	28.82	28.80	5.76
24.99	26.42	24.61	24.55	7.07
5.010	37.56	39.98	40.01	6.53
T_f = 70ºC				
T_p [ºC]	Flux (experimental) [kg/(m²·h)]	Flux (interpolated) [kg/(m²·h)]	Flux (correlations) [kg/(m²·h)]	Error (flux with correlations) [%]
5.010	66.21	67.40	67.46	1.89
10.02	64.30	63.28	63.32	1.53
15.02	61.11	58.96	58.95	3.55
20.03	60.16	54.44	54.36	9.64
24.99	48.06	49.77	49.63	3.26
5.010	66.21	67.40	67.46	1.89

Table A.3B. Comparison of the estimated flux values (using pure saturated water properties and correlations) with the experimental fluxes, for T_f temperatures of 50, 70 and 90ºC. (cont.)

T_f = 90ºC				
T_p [ºC]	Flux (experimental) [kg/(m²·h)]	Flux (interpolated) [kg/(m²·h)]	Flux (correlations) [kg/(m²·h)]	Error (flux with correlations) [%]
5.010	97.08	96.86	97.05	0.036
10.02	91.99	92.25	92.35	0.388
15.02	89.44	87.46	87.45	2.225
20.03	88.17	82.53	82.40	6.546
25.04	74.16	77.44	77.20	4.088
5.010	97.08	96.86	97.05	0.036

A.5. Comparison of the results obtained for a salt concentration of 38g/L

Table A.4B. Comparison of the two methods (interpolation and using correlations) used to estimate DCMD module properties at a feed salt concentration of 38 g/L.

T_p = 10ºC		
T_f [ºC]	Flux (interpolated) [kg/(m²·h)]	Flux (correlations) [kg/(m²·h)]
40	24.43	23.86
50	36.10	35.03
60	48.97	47.28
70	62.72	60.22
80	77.00	73.50
90	91.58	86.86
T_p = 15ºC		
T_f [ºC]	Flux (interpolated) [kg/(m²·h)]	Flux (correlations) [kg/(m²·h)]
40	21.00	20.51
50	32.38	31.43
60	44.96	43.41
70	58.40	56.08
80	72.41	69.13
90	86.80	82.30

Table A.4B. Comparison of the two methods (interpolation and using correlations) used to estimate DCMD module properties at a feed salt concentration of 38 g/L. (cont.)

T_p = 20ºC		
T_f [ºC]	Flux (interpolated) [kg/(m²·h)]	Flux (correlations) [kg/(m²·h)]
40	17.27	16.86
50	28.39	27.55
60	40.70	39.28
70	53.90	51.72
80	67.69	64.57
90	81.84	77.54
T_p = 25ºC		
T_f [ºC]	Flux (interpolated) [kg/(m²·h)]	Flux (correlations) [kg/(m²·h)]
40	13.24	12.92
50	24.14	23.41
60	36.22	34.93
70	49.19	47.16
80	62.76	59.82
90	76.82	72.67

A.6. Results obtained in the calculation of the error of the model

Table A.5B. Numerical results of the error and deviation calculations.

Sample of values	Average error [%]	Standard deviation [-]	Mean deviation [-]
T_p = 5ºC	6.618	5.474	2.235
T_p = 10ºC	9.705	12.286	5.016
T_p = 15ºC	9.123	7.269	2.968
T_p = 20ºC	7.026	2.167	0.885
T_p = 25ºC	5.986	6.675	2.725
T_f = 50ºC	7.225	1.868	0.835
T_f = 70ºC	3.973	4.897	2.190
T_f = 90ºC	2.656	5.782	2.586
All above	6.667	6.243	0.931

Appendix C – DCMD implementation in DWSIM

A.7. Comparison of results obtained by DWSIM with experimental values

Table A.1C. Comparison of fluxes obtained by DWSIM with experimental results, for T_p temperatures of 5, 10, 15, 20 and 25ºC.

T_p = 5ºC			
T_f [ºC]	Flux (experimental) [kg/(m²·h)]	Flux (correlations) [kg/(m²·h)]	Flux (DWSIM) [kg/(m²·h)]
40.40	24.41	28.43	27.99
50.63	37.63	40.82	40.04
60.41	51.19	53.87	53.37
70.19	64.41	67.73	67.58
80.57	80.00	82.99	82.32
90.21	97.97	97.39	97.32
T_p = 10ºC			
T_f [ºC]	Flux (experimental) [kg/(m²·h)]	Flux (correlations) [kg/(m²·h)]	Flux (DWSIM) [kg/(m²·h)]
39.94	18.56	24.80	24.87
50.02	32.82	36.60	36.61
59.96	47.73	49.46	49.59
70.04	65.97	63.39	63.45
79.98	82.21	77.66	77.89
90.06	92.49	92.44	92.63
T_p = 15ºC			
T_f [ºC]	Flux (experimental) [kg/(m²·h)]	Flux (correlations) [kg/(m²·h)]	Flux (DWSIM) [kg/(m²·h)]
40.02	17.63	21.44	21.43
50.04	28.90	32.88	32.87
60.06	49.42	45.53	45.54
70.08	61.27	59.07	59.10
80.10	76.59	73.18	73.26
90.11	90.75	87.64	87.77

Table A.1C. Comparison of fluxes obtained by DWSIM with experimental results, for T_p temperatures of 5, 10, 15, 20 and 25ºC. (cont.)

T_p = 20ºC			
T_f [ºC]	Flux (experimental) [kg/(m²·h)]	Flux (correlations) [kg/(m²·h)]	Flux (DWSIM) [kg/(m²·h)]
40.02	17.09	17.68	17.68
50.04	30.61	28.87	28.86
60.06	45.15	41.24	41.25
70.08	60.20	54.49	54.54
80.10	73.72	68.34	68.45
90.11	89.29	82.56	82.75
T_p = 25ºC			
T_f [ºC]	Flux (experimental) [kg/(m²·h)]	Flux (correlations) [kg/(m²·h)]	Flux (DWSIM) [kg/(m²·h)]
40.09	11.54	13.72	13.64
50.05	26.37	24.61	24.59
60.15	36.81	36.82	36.73
70.11	48.35	49.76	49.78
80.07	66.21	63.33	63.46
90.04	75.00	77.29	77.57

Appendix D – DCMD pilot plant

Table A.1D. Dimensions of steel tubes that follow the ASME B 36.10M standard.

Nominal pipe size [inch]	Nominal diameter [mm]	Outside diameter [mm]	Wall thickness SCH 40 [mm]
1	25	33.4	3.38
2	50	60.3	3.91
3	80	88.9	5.49
4	100	114.3	6.02
5	125	141.3	6.55
6	150	168.3	7.11
8	200	219.1	8.18
10	250	273.1	9.27

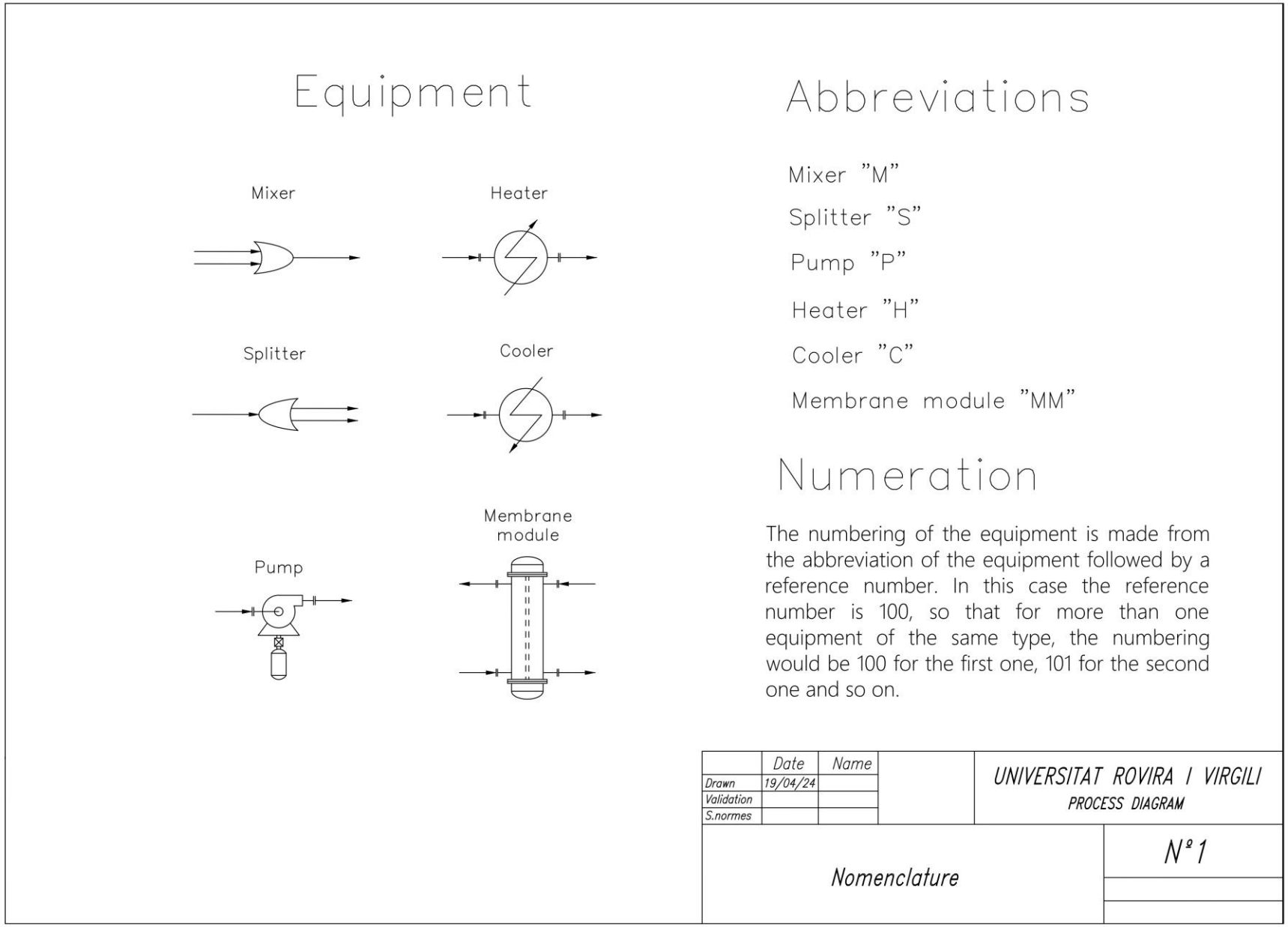

Figure A.1D. Nomenclature and numeration followed in the DCMD pilot plant sizing and in the process flow diagram.

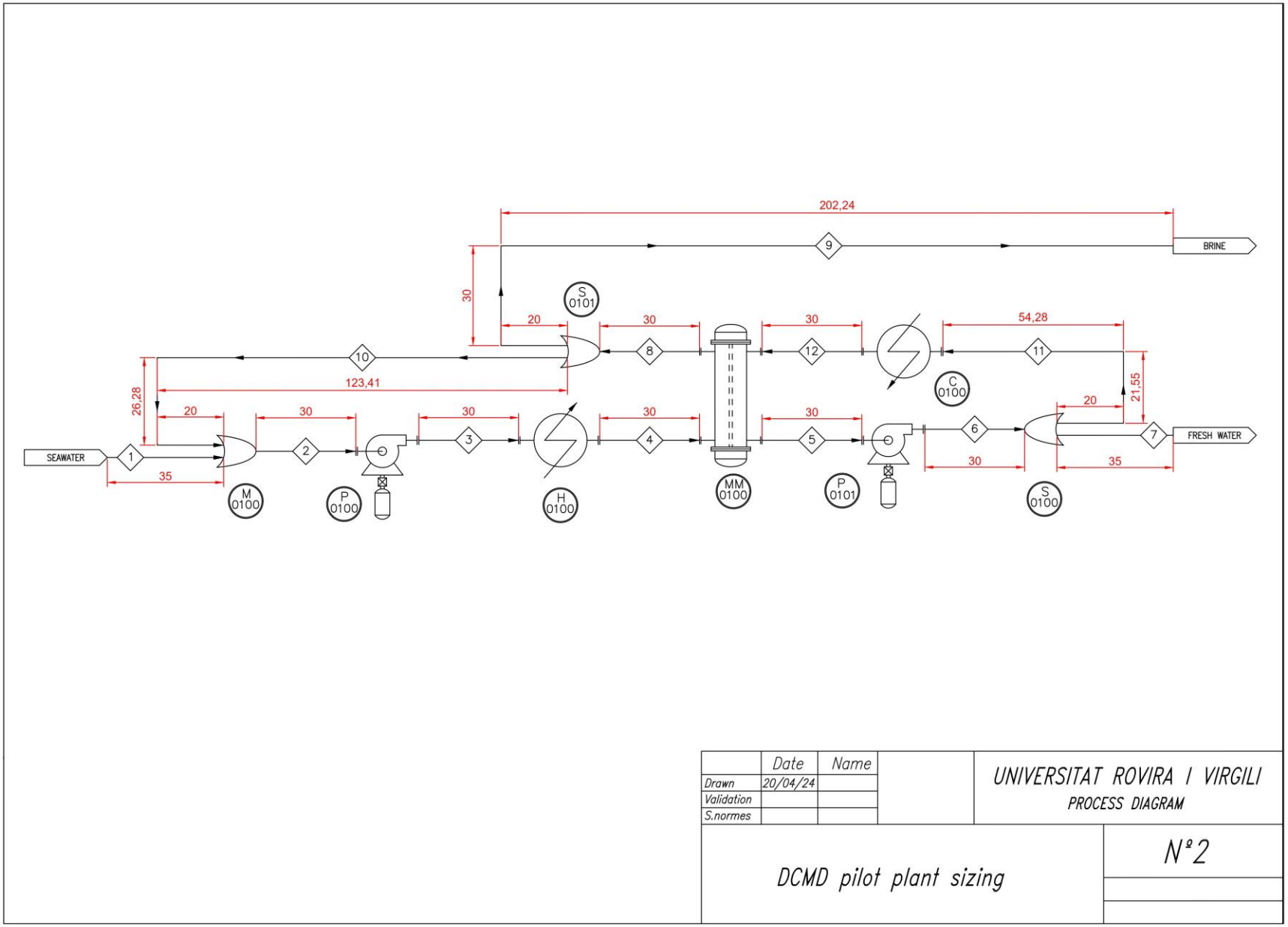

Figure A.2D. DCMD pilot plant sizing.

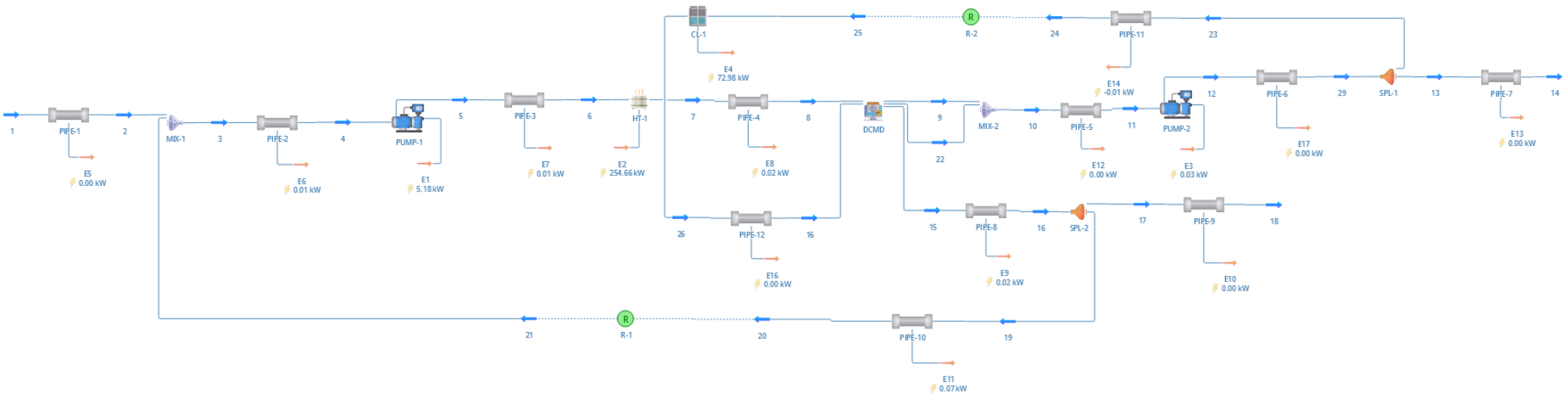

Figure A.3D. Schematic of a DCMD system in DWSIM considering the head and heat loss in the pipes.

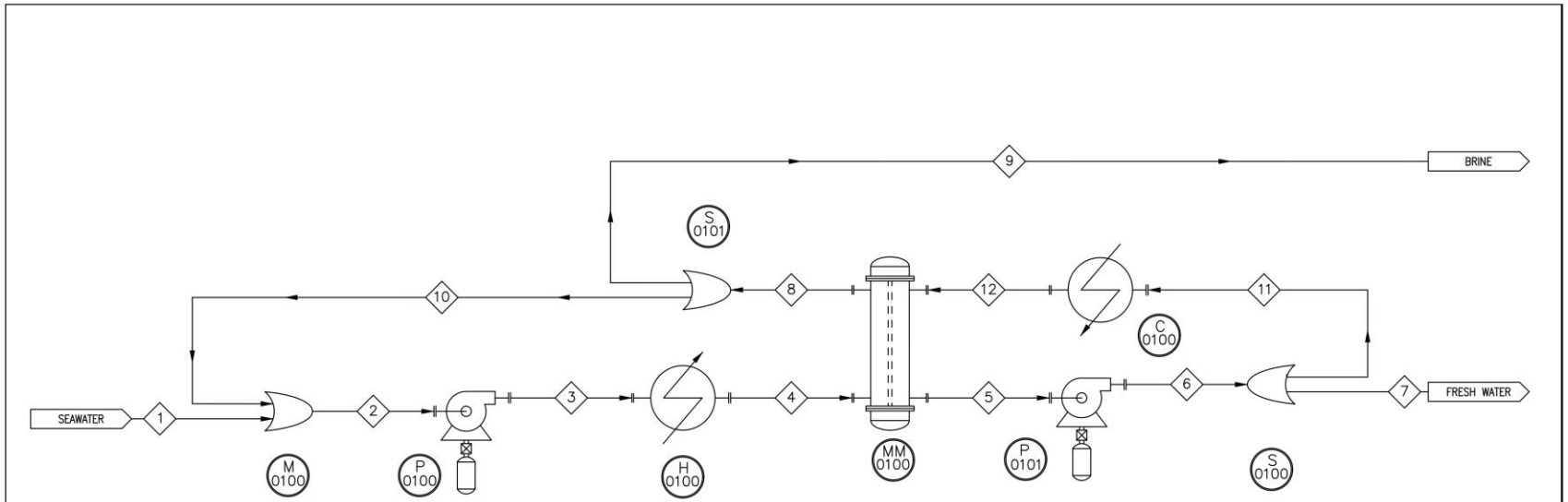

Stream	1	2	3	4	5	6
Temperature, °C	25.0	89.2	89.2	90.0	10.8	10.8
Pressure, Pa	101325	100258	150000	149948	148981	150000
Mass flow, kg/s	1.00	78.22	78.22	78.22	22.00	22.00
Water	0.96	74.41	74.41	74.41	~ 22.00	~ 22.00
Salt	0.04	3.81	3.81	3.81	~ 0.00	~ 0.00
Mass fraction						
Water	0.962	0.951	0.951	0.951	~ 1.00	~ 1.00
Salt	0.038	0.049	0.049	0.049	1.943E−5	1.943E−5

Stream	7	8	9	10	11	12
Temperature, °C	10.8	90.0	90.0	90.0	10.8	10.0
Pressure, Pa	149950	149898	149848	149848	149950	149031
Mass flow, kg/s	0.22	78.00	0.78	77.22	21.78	21.78
Water	~ 0.22	74.19	0.74	73.45	~ 21.78	~ 21.78
Salt	~ 0.00	3.81	0.04	3.77	~ 0.00	~ 0.00
Mass fraction						
Water	~ 1.00	0.951	0.951	0.951	~ 1.00	~ 1.00
Salt	1.943E−5	0.049	0.049	0.049	1.943E−5	1.943E−5

	Date	Name	
Drawn	21/04/24		
Validation			
S.normes			

UNIVERSITAT ROVIRA I VIRGILI
PROCESS DIAGRAM

DCMD Process Flow Diagram

Nº3

Figure A.4D. DCMD Process Flow Diagram.

Appendix E – Self -Evaluation Questionnaire

a) Evaluate the acquired **competences** according to the **tasks** you have carried out.

Degree Competences		**Task in which you have observed the competence**	**Self evaluation [Rank 1 to 10]**	**Aspects to be improved**
SPECIFIC COMPETENCES				
A1.1	Effectively apply knowledge of basic, scientific and technological materials pertaining to engineering.	In the selection of pipe material	9	
A1.2	Design, execute and analyze experiments related to engineering	In the simulation environment and energy optimization	9	
A1.3	Be able to analyze and synthesize the continuous progress of products, processes, systems and services, whilst applying criteria of safety, economic viability, quality and environmental management. (G6)		-	
A1.4	Know how to establish and develop mathematical models by using the appropriate software in order to provide the scientific and technological basis for the design of new products, processes, systems and services and for the optimization of existing ones. (G5)	In the implementation of the mathematical model to the DWSIM software	10	
A2.1	Be able to apply the scientific method and the principles of engineering and economics to formulate and solve complex problems that arise in processes, equipment, installations and services, in which the material undergoes changes to its composition, state or energy content, these changes being characteristic of industrial chemistry and other related sectors such as pharmacology, biotechnology, materials sciences, energy, food and the environment. (G1)	In the study of the variation of the concentration for the energetically optimal operating conditions	8	
A2.2	Conceive, project, calculate and design processes, equipment, industrial installations and services in the field of chemical engineering and related industrial sectors in terms of quality, safety, economics, the rational and efficient use of natural resources and the conservation of the environment. (G2)		-	
A2.3	Lead and technically and economically manage projects, installations, plants, companies and technological centres in the ambit of chemical engineering		-	

	and related industrial sectors. (G3)			
A3.1	Apply knowledge of mathematics, physics, chemistry, biology and other natural sciences by means of study, experience, practice and critical reasoning in order to establish economically viable solutions for technical problems (I1).	In the conclusion offered by the project carried out	8	
A3.2	Design and optimize products, processes, systems and services for the chemical industry on the basis of various areas of chemical engineering, including processes, transport, separation operations, and chemical, nuclear, elctrochemical and biochemical reactions engineering (I2).	On energy optimization in the operation conditions of the desalination plant	9	
A3.3	Conceptualize engineering models and apply innovative problems solving methods and appropriate IT applications to the design, simulation, optimization and control of processes and systems (I3).	In the global elaboration of the project	8	
A3.4	Be able to solve unfamiliar and ill-defined problems by taking into account all possible solutions and selecting the most innovative. (I4)	In the implementation of the Python code in the DWSIM simulator	9	
A3.5	Lead and supervise all types of installation, process, system and service in the different industrial areas related to chemical engineering (I5).		-	
A3.6	Design, construct and implement methods, processes and installations for the integrated management of waste, solids, liquids and gases, whilst also taking into account the impacts and risks of these products (I6).		-	
A4.1	Lead and organize companies and production and service systems by applying knowledge and abilities regarding industrial organization, commercial strategy, planning and logistics, mercantile and labour legislation, and financial and costs accounting (P1).		-	
A4.2	Lead and manage the organization of work and human resources by applying criteria regarding industrial safety, quality management, occupation risk prevention, sustainability and environmental management (P2).		-	
A4.3	Manage research, development and technological innovation whilst ensuring the transfer of technology and taking into account property and patent rights (P3).	In the overall development of the project	8	
A4.4	Adapt to structural changes in society caused by economic, energy or natural factors so as to be able to solve any resulting problems and to contribute technological solutions with a high	In the overall development of the project	9	

	commitment to sustainability (P4).			
A4.5	Lead and monitor the control of installations, processes, products, certification, auditing, verification, testing and reports (P5).		-	
A5.1	Carry out, present and defend (once all the curriculum credits have been obtained) an original individually produced piece of work before a university panel. The work will consist of a professional integrated Chemical Engineering project that synthesizes (TFM1)		9	
TRANSVERSAL COMPETENCES				
B1.1	Communicate and discuss proposals and conclusions in a clear and unambiguous manner in specialized and non-specialized multilingual forums (G9).	In the follow-up meetings held	8	
B1.2	Adapt to changes and be able to apply new and advanced technologies and other important developments with initiative and entrepreneurial spirit. (G10)	In the implementation of the Python code in the DWSIM simulator	8	
B2.1	Lead and define multidisciplinary teams that are able to make technical changes and address management needs in national and international contexts. (G8)		-	
B3.1	Work in a team with responsibilities shared among multidisciplinary, multilingual and multicultural teams		-	
B4.1	Be able to learn autonomously in order to maintain and improve the competences pertaining to chemical engineering that enable continuous professional development. (G11)	In learning the Python programming language autonomously	9	
B5.1	Carry out and lead the appropriate research, design and development of engineering solutions in new or little understood areas, whilst applying criteria of creativity, originality, innovation and technology transfer. (G4)	In the search for bibliographical information	8	
B5.2	Bring together knowledge, make judgements and take decisions on the basis of incomplete or limited knowledge whilst taking into account the social and ethical responsibilities of professional practice. (G7)	In the assumptions made in the validation of the model	9	
NUCLEAR COMPETENCES				
C1.1	Have an intermediate mastery of a foreign language, preferably English	In the drafting of the project	8	
C1.2	Be advanced users of the information and communication technologies	In the search for bibliographical information	9	
C1.3	Be able to manage information and knowledge	In the search for bibliographical information	9	
C1.4	Be able to express themselves correctly both orally and in writing in one of the two official languages of the URV	In the follow-up meetings held	9	

C2.1	Be committed to ethics and social responsibility as citizens and professionals	In the overall development of the project	10	
C2.2	Be able to define and develop their academic and professional project	In the overall development of the project	10	

b) Evaluate the final master project and suggest improvements.

Key steps	**Evaluation [Mark 1 to 10]**	**Improvement proposed**
Selection/assignment of the project (dissemination, communication, assignment requirements...)	10	
Stay (welcome, length, relationship, follow-up made by the company...)	10	
Follow-up made by URV tutor	10	
Other aspects to be considered (which ones...)	-	